DEAD box RNA helicases 5 and 17 are new host factors for Sindbis virus infection

Mélanie Messmer [1], Louison Pierson [1], Charline Pasquier [1], Nikola Djordjevic [1], Johana Chicher [2], Philippe Hammann [2], Sébastien Pfeffer [1], Erika Girardi [1]

[1] Université de Strasbourg, Architecture et Réactivité de l'ARN, Institut de Biologie Moléculaire et Cellulaire du CNRS, 2 allée Konrad Roentgen, 67084 Strasbourg France.

[2] Université de Strasbourg, Institut de Biologie Moléculaire et Cellulaire du CNRS, Plateforme Protéomique Strasbourg – Esplanade, 2 allée Konrad Roentgen, 67084 Strasbourg France.

* To whom correspondence should be addressed: e.girardi@ibmc-cnrs.unistra.fr.

Abstract

The DEAD-box ATP-dependent RNA helicases DDX5 and DDX17 play an important role in many aspects of cellular RNA biology, including metabolism, translation, splicing, transcriptional regulation, ribosome biogenesis and mRNA nuclear export. Both RNA helicases were also found to either promote or inhibit viral replication upon infection with several RNA viruses. Here we show that DDX5 depletion by RNAi or CRISPR/Cas9 has a negative impact on Sindbis virus (SINV) infection at the viral protein, RNA and infectious particle accumulation level, indicating a pro-viral role. We also demonstrate that DDX5 interacts with the SINV RNA in infected conditions. Furthermore, proteomic analysis of the DDX5 interactome in mock and SINV-infected HCT116 cells identified new cellular and viral partners and confirmed the interaction between DDX5 and DDX17. Of note, while DDX5 and DDX17 are mostly nuclear in uninfected cells, they both re-localize to the cytoplasm upon SINV infection and interact with the viral capsid protein. Finally, we show that DDX17 depletion has a negative impact on SINV and further reduces viral infection in a DDX5-depleted background, suggesting a cumulative pro-viral effect of the DDX5 and DDX17 proteins on SINV. These results not only expand our understanding of the roles played by DDX5 and DDX17 as regulators of viral infections, but also highlight their critical contributions to the SINV life cycle.

Keywords: DDX5, DDX17, helicase, RNA, Sindbis virus

1. Introduction

DEAD box RNA helicases play crucial molecular functions in virtually all aspects of RNA metabolism, including transcription, pre-mRNA splicing, RNA transport, rRNA biogenesis and RNA decay (Tanner and Linder, 2001). These enzymes can structurally remodel short RNA duplex molecules and rearrange RNA-protein interactions in an ATP-dependent fashion. The DEAD-box RNA helicase family is characterized by the presence of specific highly conserved motifs, including the Asp–Glu–Ala–Asp (D-E-A-D) box within the catalytic core (Linder and Jankowsky, 2011) from which this family gets its name. Recently, DEAD box RNA helicases have emerged as pivotal host factors upon viral infection that act by either modulating antiviral signalling pathways or by directly recognizing viral RNA and acting at different steps of the viral life cycle (Bonaventure and Goujon, 2022; Meier-Stephenson et al., 2018; Taschuk and Cherry, 2020).

The multifunctional DEAD-box RNA helicase DDX5 (also known as p68) is an essential splicing factor (Lin et al., 2005; Liu, 2002) involved in many other aspects of cellular RNA metabolism (Xing et al., 2019). Within the DDX gene family members, DDX5 exhibits the highest degree of homology with DDX17 (also known as p72) (Janknecht, 2010). These two proteins can form homodimers but are preferentially associated in hetero-dimers (Ogilvie et al., 2003). DDX5 and DDX17 exhibit partially overlapping functions, including involvement in transcriptional regulation (Giraud *et al*, 2018), alternative splicing modulation (Dardenne et al., 2014) and ribosomal biogenesis (Jalal et al., 2007).

A growing body of evidence suggests that DDX5 and DDX17 play crucial roles during viral infection (Cheng et al., 2018; Hu et al., 2022). Despite their known function as a heterodimer, these two proteins exhibit distinct functions in response to specific viral infections. For instance, depletion of DDX17 but not of DDX5 increases infection of Rift Valley Fever virus (RVFV), a segmented, negative-sense RNA virus. In particular, DDX17 binding to a stem-loop structure in the viral RNA is sufficient to trigger the antiviral effect (Moy et al., 2014).
Moreover, the same protein can have either a positive or a negative effect on different viruses. While DDX5 is antiviral in response to DNA viruses such as hepatitis B virus (HBV) (Zhang et al., 2016) or myxoma virus (MYXV) (Rahman et al., 2017), it acts as a positive cofactor of the Human Immunodeficiency Virus 1(HIV-1) proteins Rev and Tat facilitating viral

replication (Sithole et al., 2020; Zhou et al., 2013). Interestingly, several positive, single-stranded RNA viruses with a cytoplasmic replication cycle have also evolved to hijack DDX5 and favour their own replication. DDX5 was also shown to be pro-viral for hepatitis C virus (HCV) (Goh et al., 2004; Ríos-Marco et al., 2016), severe acute respiratory syndrome coronavirus (SARS-CoV) (Chen et al., 2009), japanese encephalitis virus (JEV) (Li et al., 2013) and porcine reproductive and respiratory syndrome virus (PRRSV) (Zhao et al., 2015). In most cases DDX5 promotes viral replication through direct interaction with specific viral proteins and/or viral RNA.

In a previous study we identified DDX5 as one of the factors associated with the Sindbis virus (SINV) replication complex by dsRNA-IP coupled to mass spectrometry (DRIMS) approach (Girardi et al., 2023). Moreover, we observed that DDX5 knockdown (KD) significantly reduces GFP expression in HCT116 cells infected with a GFP-expressing SINV by quantification of GFP fluorescence intensity (Girardi et al., 2023). SINV is a small, enveloped, arthropod-borne virus which belongs to the *Alphavirus* genus from the *Togaviridae* family. Alphaviruses are widely distributed viruses (Weaver and Barrett, 2004) that pose a re-emerging threat to human health due to their potential to cause severe arthritogenic and neurological diseases and for which approved vaccines are not yet available. Most of our understanding on the alphavirus life cycle derives from research on the prototypical model SINV. The virus possesses a positive, single-stranded genomic RNA of approximately 11 kb, capped and polyadenylated, organized into two distinct open reading frames (ORFs). The first ORF encodes the non-structural proteins (nsP1, nsP2, nsP3 and nsP4) necessary for viral RNA replication. An antigenomic RNA accumulates in the cytoplasm and serves as a template for the synthesis of both genomic and sub-genomic RNA. The second ORF is translated from the sub-genomic RNA and gives rise to the structural proteins (Capsid, E3, E2, 6K and E1) needed for viral particle assembly (Griffin, 2007).

In this study we investigated the effect of the human RNA helicases DDX5 and DDX17 on SINV. We demonstrated that knocking down and knocking out DDX5 strongly reduces SINV replication in human HCT116 cells. We observed that DDX5 is able to interact with both the viral RNA and the viral capsid protein in the cytoplasm of infected cells. We determined the interactome of DDX5 by proteomic analysis in uninfected and SINV infected conditions and identified new and previously known DDX5 partners. We validated by co-immunoprecipitation analysis that DDX5 interacts with DDX17 and re-localizes to the cytoplasm upon SINV

infection. Finally, we also demonstrated that knockdown of DDX17 has a negative impact on SINV infection and that DDX17 depletion in *DDX5* knockout cells show a greater decrease in virus replication, indicating a cooperation between DDX17 and DDX5 in promoting SINV infection.

2. Materials and methods

2.1. Cell lines and viruses

HCT116, BHK21 and Vero E6 cells were maintained at 37°C in a humidified atmosphere containing 5% CO_2 and cultured in Dulbecco's Modified Eagle medium (DMEM; Invitrogen) supplemented with 10% FBS. Viral stocks were prepared from infectious clones (kindly provided by Dr Carla Saleh, Institut Pasteur, Paris, France) carrying either the wild-type or a GFP containing version of the SINV genomic sequence as previously described in (López et al., 2020). Briefly, the plasmids were linearized by XhoI digestion and used as a substrate for *in vitro* transcription using the mMESSAGE mMACHINE capped RNA transcription kit (Ambion, Thermo Fisher Scientific Inc.). In vitro synthesized viral RNA was transfected in BHK21 cells, viral infectious particles were collected 48 hpt and used to infect BHK21 for the full viral production. Titers were measured by standard plaque assay in Vero E6 cells. Cells were infected at a MOI of 1, 10^{-1} or 10^{-2} as indicated in the figure legends.

2.2. Plaque assay

For plaque assay, 1 million Vero E6 cells were seeded in a 96 well plate and infected for 1 hour with viral supernatants prepared in 10-fold dilution cascade. After removal of the viral inoculum, 2.5% carboxymethyl cellulose diluted in DMEM-FBS10% was added and cells were incubated at 37ºC in a humidified atmosphere of 5% CO2. Plaques were counted manually under the microscope after 72 h.

2.3. DDX5 CRISPR/Cas9 knockout

Guide RNA (gRNA) sequences targeting the human DDX5 gene were designed using the CRISPOR tool (http://crispor.tefor.net) and cloned into the pX459-V2 vector (Addgene Plasmid #62988 was a gift from Feng Zhang (Ran et al., 2013)). Briefly 0.25 µM of the annealed oligos and 100 ng of digested vector were ligated and transformed into DH5 alpha cells.

guideRNA#2 DDX5 sense: 5' CACCGATAATAGGGTGTTCATAGGT 3'
guideRNA#2 DDX5 antisense: 5' AAACACCTATGAACACCCTATTATC 3'
guideRNA#1 DDX5 sense: 5' CACCGCCCTACTTCCTCCAAATCG 3'

guideRNA#1 DDX5 antisense: 5’ AAACCGATTTGGAGGAAGTAGGGC 3’

HCT116 cells were transfected with 2 plasmids containing the sequence of gRNA#1 and #2, respectively. Twenty-four hours post-transfection, cells were treated with 1 µg/mL puromycin for 48h. Surviving cells were diluted to obtain 0.5 cells/ well in 96 well plates. Two weeks later, cellular genomic DNA was extracted from individual colonies. Cells were lysed in genomic DNA extraction buffer (50 mM Tris-HCl [pH 8.0]; 100 mM EDTA [pH 8.0], 100 mM NaCl, 1% SDS) containing 0.1 mg of proteinase K and incubated overnight at 55°C. Then, 50 ng of genomic DNA were amplified with the GoTaq (Promega) using specific primers (IDT) to detect the deletion (DDX5 FW: 5’-ATAAATCCCCGGCTTCCGAC-3’; DDX5 RV: 5’-AGAGGGGGTAGGTGGAAACAA-3’). Wild type genomic DNA was used as control template. PCR reactions were loaded on a 1 % agarose gel and the obtained amplicons were gel purified and sequenced by Sanger sequencing.

2.4. SiRNA-based knockdown

For the knockdown experiments, 0.6 millions of cells HCT116 cells were reverse-transfected with 20nM of ON-TARGETplus Human siRNAs (Horizon) against DDX5 (L-003774-00-0005), DDX17 (L-013450-01-0005) or non-targeting Control Pool (D-001810-10-05) using the Lipofectamine 2000 transfection reagent (Thermo Fisher Scientific, #11668019) according to the manufacturer’s instructions in 6 well plates. After 24 hours, cells were transfected again with 20nM of the same mix of siRNAs and incubated overnight. Cells were then infected with SINV-GFP at a MOI of 0.1 for 24 hours. Supernatant were collected for plaque assay experiment and proteins and RNA were collected for western blot and RT-qPCR analyses, respectively.

2.5. Live-cell imaging

Two-hundred thousand WT and *DDX5* KO HCT116 cells were seeded in 12 well plate and infected with SINV-GFP at MOI 1, 0.1 or 0.01. Uninfected cells were used as control. GFP fluorescence and phase contrast were observed using a CellcyteX live-cell imaging system (Discover Echo). Six images per well (10X objective) were acquired every 6 hours for 72hrs and were analysed with the Cellcyte Studio software to determine cell confluency and GFP relative intensity.

2.6. Cloning

Amplicons containing the coding sequence for the individual viral proteins were generated by PCR from the plasmid carrying the SINV genomic sequence (kindly provided by Dr. Carla Saleh, Institut Pasteur, Paris, France) and cloned into the pDONOR221 vector (Invitrogen) by recombination using the Gateway BP clonase (Invitrogen) according to the manufacturer instructions. The pDEST-FLAG-HA- nsP1, pDEST-FLAG-HA- nsP2, pDEST-FLAG-HA- nsP3, pDEST-FLAG-HA- nsP4 and pDEST-FLAG-HA- capsid vectors were obtained by recombination using Gateway LR clonase (Invitrogen) in the pDEST- FLAG-HA vector according to the manufacturer instructions, as in (Montavon et al., 2021).Primers used for the PCR are listed below:

pDONR NSP1 FW
5’ GGGGACAAGTTTGTACAAAAAAGCAGGCTTCGAGAAGCCAGTAGTAAAC-3’
pDONR NSP1 REV
5’-GGGGACCACTTTGTACAAGAAAGCTGGGTCTTATTTGCTCCGATGTCCG-3’
pDONR NSP2 FW
5’GGGGACAAGTTTGTACAAAAAAGCAGGCTTCGCATTAGTTGAAACCCCG-3’
pDONR NSP2 REV
5’GGGGACCACTTTGTACAAGAAAGCTGGGTCTTATTGGCTCCAACTCCATCTC-3’
pDONR NSP3 FW
5’-GGGGACAAGTTTGTACAAAAAAGCAGGCTTCGCGCCGTCATACCGCACC-3’
pDONR NSP3 REV
5’-GGGGACCACTTTGTACAAGAAAGCTGGGTCTTATTGTATTCAGTCCTCC-3’
pDONR NSP4 FW
5’-GGGGACAAGTTTGTACAAAAAAGCAGGCTTCCTAACCGGGGTAGGTGGGTAC 3’
pDONR NSP4 REV
5’GGGGACCACTTTGTACAAGAAAGCTGGGTCTTACTATTTAGGACCACCGTAGAG-3’
pDONR capsid FW
5’-GGGGACAAGTTTGTACAAAAAAGCAGGCTTCAATAGAGGATTCTTTAAC-3’
pDONR capsid REV
5’-GGGGACCACTTTGTACAAGAAAGCTGGGTCTTATTCCACTCTTCTGTCC-3’

2.7. Flag-HA SINV protein co-IP

For the experiment, 0.6 million of HCT 116 cells were seeded in 6 well plates. The following day 3µg of the pDEST-HA-FLAG described above were transfected using the Lipofectamine 2000 transfection reagent as per manufacturer's recommendations. 48 hours later, the cells were washed once with 1xPBS and lysed in 600 µL of Miltenyi lysate buffer (50 mM Tris-HCl pH 7.5, 140 mM NaCl, 1.5 mM $MgCl_2$, 0.1% NP-40), supplemented with Complete-EDTA-free Protease Inhibitor Cocktail (Merck). Cells were lysed for 30 min incubation on ice and debris were removed by 10 min centrifugation at 10,000g at 4°C. An aliquot of the cleared lysates (50 µL) was kept aside as protein Input. Samples were divided into equal parts (250 µL each) and incubated with 50 µL of magnetic microparticles coated with monoclonal HA or MYC antibodies (MACS purification system, Miltenyi Biotec) at 4°C for 1 hour under rotation (10 rpm). Samples were passed through µ Columns (MACS purification system, Miltenyi Biotec). The µ Columns were then washed 4 times with 200 µL of WASH buffer1 and 1 time with 200 µL of WASH buffer 2. To elute the immunoprecipitated proteins, 70µL of 95°C pre-warmed 2x Western blot loading buffer (10% glycerol, 4% SDS, 62.5 mM Tris-HCl pH 6.8, 5% (v/v) 2-β-mercaptoethanol, Bromophenol Blue) was passed through the µ Columns. Proteins were analysed by western blotting.

2.8. DDX5 and DDX17 co-immunoprecipitation and RNA immunoprecipitation

DDX5 and DDX17 immunoprecipitations (IP) were performed as in (Girardi et al., 2023) with some modifications. Briefly, 4 millions of mock or SINV-GFP infected HCT116 cells (MOI 0.1, 24 hpi) were lysed using RIP immunoprecipitation buffer (50mM tris-HCL [pH 7.5], 150mM NaCl, 5 mM EDTA, 0.05% SDS, 1% triton, 1 tablet of commercial protease inhibitor cocktail (Merck)). DNase treatment was performed on the lysates by adding 1µL of RNAse-free DNase I (Thermo Fisher Scientific), 10mM MgCl2, 5mM Cacl2 and 1µL of Ribolock (Thermo Fisher Scientific) to the 1 mL lysate and incubating for 20 min at 37°C. Lysates were centrifuged for 10 min at 4°C. Supernatants were collected and pre-cleared for 1h at room temperature with Dynabeads protein G magnetics beads (Invitrogen) blocked with yeast tRNA (Invitrogen). Lysates were incubated over night at 4°C with 40 µL of Dynabeads protein G beads conjugated with 2 µg rabbit anti-DDX5 antibody (ab21696; abcam), or rabbit anti-DDX17 antibody (19910-1-AP, Proteitech) or 2µg rabbit IgG antibody (2729; Cell Signaling Technology). Beads were washed 3 times with RIP buffer containing 150mM NaCl, twice with

the same buffer supplemented with 50mM of NaCl, and 3 times 3 times with RIP buffer containing 150mM NaCl. 30% of the immunoprecipitated protein and 70% of the associated RNA were eluted with Laemmli 1X at 95°C for 10 min or with 1 mL TriReagent (Thermo Fisher Scientific), respectively. Proteins were analysed by western blot or by mass spectrometry, while RNA was extracted and analysed by RT-qPCR.

2.9. Western Blot

Cells were collected in 300 to 500 µL of lysis buffer (50mM tris-HCL [pH 7.5], 150mM NaCl, 5 mM EDTA, 0.05% SDS, 1% triton, 1 tablet of commercial protease inhibitor cocktail (ROCHE)) and incubated for 30 min on ice. Cell lysates were then collected and protein concentration was determined using the Bradford method (Bio-Rad). For total protein analysis, 20µg of protein samples were heated in 1X Laemmli buffer at 95°C for 5 min and loaded on pre-cast 4-20% SDS-polyacrylamide electrophoresis gel (Bio-Rad). For the RIP experiment, 0.5 % of input and 12,5% of immunoprecipitated protein were used. After migration, the proteins were transferred onto 0.45 µm nitrocellulose membranes (GE healthcare). The membranes were blocked with 5% non-fat milk diluted in PBS 1X (Euromedex) complemented with 0.2% Tween-20 (PBS-T) for 1 h at room temperature and then were incubated at 4°C overnight or 1 h at room temperature with the following specific primary antibodies: anti-DDX5 (mouse- horseradish peroxidase(HRP), sc-365164; Santa Cruz Biotechnology) or anti-DDX5 (rabbit, ab21696; Abcam), anti-DDX17 (mouse, sc-271112; Santa Cruz Biotechnology), anti-tubulin HRP (ab21058; Abcam), anti-GAPDH-HRP (mouse, ab9482; Abcam), anti-capsid (rabbit, kind gift of Diane Griffin), anti-GFP (mouse, 11814460001, Roche). Membranes were washed 3 times with PBS-T for 5 min and incubated with mouse-HRP (A4416; Merck) and rabbit-HRP (GENA9640V, Merck) secondary antibodies for 1 h at room temperature. Proteins were detected using the Chemiluminescence substrate (Supersignal West Pico; Pierce) and analysed with the Fusion FX imaging system (Vilber).

2.10 RNA extraction and RT-qPCR

Total RNA and RNA enriched upon specific protein immunoprecipitation (RIP) were extracted using TriReagent (Invitrogen, Thermo Fisher Scientific) according to the manufacturer's instructions. For total RNA analysis, 1 µg of RNA was reverse transcribed with the SuperScript VILO Master Mix (Invitrogen, Thermo Fisher Scientific) according to the manufacturer’s instructions. For the RIP experiment, 1 µL of samples before and after IP was used for retro-

transcription using the same protocol. RT-qPCR was performed on cDNA using the Maxima SYBR Green qPCR Master Mix K0253; Thermo Fisher Scientific) on the CFX96 touch Real-Time PCR machine (Bio-Rad) using the following primers at an annealing temperature of 60°C:

SINV genome FW: `
5′-CCACTACGCAAGCAGAGACG-3′;
SINV genome RV:
5′-AGTGCCCAGGGCCTGTGTCCG-3′;
GAPDH FW:
5′-CTTTGGTATCGTGGAAGGACT-3′;
GAPDH RV:
5′-CCAGTGAGCTTCCCGTTCAG-3’
SINV subgenome-genome FW
5’CCACAGATACCGTATAAGGCA 3’
SINV subgenome-genome RV
5’ TGCAGGTAATGTACTCTTGG 3’
OAS3 FW:
5’ TGCTGCCAGCCTTTGACGCC 3’
OAS3 RV:
5’ TCGCCCGCATTGCTGTAGCTG 3’

2.10. Immunostaining

Mock or SINV WT- infected cells were plated on 8 wells LabTek slide (Merck Millipore), were fixed with 4% formaldehyde (Merck) diluted in PBS 1X for 10 min at room temperature and then washed 3 times with PBS 1X. Cells were blocked in blocking buffer (0.1% Triton X-100; PBS 1 X; 5% normal goat serum) for 1 h. The following primary antibodies were diluted 1:400 in blocking buffer and incubated over night at 4°C: mouse anti-dsRNA J2 (RNT-SCI-10010200; Jena bioscience), mouse anti- DDX5 (67025 Proteintech) or rabbit anti-DDX5 (ab21696; Abcam), anti-DDX17 (mouse, sc-27112; Santa Cruz Biotechnology), anti-capsid (rabbit, kind gift of Diane Griffin). Cells were washed with PBS 1X-Triton 0.1%. and incubated for 1 h at room temperature with secondary antibodies (goat anti-mouse Alexa 594 (A11032, Invitrogen) or goat anti-rabbit Alexa 488 (A11008, Invitrogen) secondary antibodies) diluted at 1:1000 in PBS 1X-Tween 0.1%. DAPI staining was performed for 5 min in PBS 1X to reveal the nuclei (D1306, Invitrogen, Thermo Fisher Scientific). Slides were mounted on coverslips

with Fluoromount-G mounting media (Invitrogen, Thermo Fisher Scientific) and observed by confocal microscopy (LSM780, Zeiss). Images were analysed using Image J software.

2.11. Sequential immunostaining and FISH

Mock or SINV-WT infected (MOI 1, 24hpi) HCT116 cells were grown on 18 mm round cover glass in 12-well cell culture plates.

Cells were fixed with 3.7 % formaldehyde diluted in PBS 1X for 10 min at room temperature. Cells were then permeabilized in 1mL of 0.1% Triton X-100 in 1X PBS for 5 min at room temperature and incubated with anti-DDX5 primary antibody (rabbit, ab21696; Abcam) diluted to 1:400 in PBS 1X for 1 hour. Goat anti-rabbit Alexa 488 (A11008, Invitrogen) secondary antibody diluted to 1:1000 was added on the cells for 1 hour at room temperature.

Cells were fixed again with 3.7 % formaldehyde (Biosearch technologies) diluted in PBS 1X for10 min at room temperature and incubated over night at room temperature with the SINV genome specific LGC Biosearch Technologies' Stellaris® RNA FISH Probe diluted in RNA FISH hybridization buffer (Stellaris, Biosearch technologies). DAPI staining was performed for 30 min to reveal the nuclei (D1306, invitrogen, Thermo Fisher Scientific). Slides were mounted on coverslips with Fluoromount-G mounting anti-fading media (Invitrogen, Thermo Fisher Scientific) and observed by confocal microscopy (LSM780, Zeiss). Images were analysed using Image J software.

2.12. Statistical analysis

Statistical analyses were performed using GraphPad Prism 9 software using the test recommended by the software. Generally, a paired Student’s t test was performed for comparisons between two samples for plaque assays and a one-sample t test was performed to determine the significance of the fold change on qPCR results. The number of replicates per experiment and the specific statistical tests used are stated in the figure legends.

2.13. Mass spectrometry analyses

For LC-MS/MS analyses, proteins were prepared as described in a previous study (Girardi et al., 2023). Proteins eluted from the beads were washed with 2 sequential overnight precipitations with glacial 0.1 M ammonium acetate in 100% methanol (5 volumes) followed by 3 washes with glacial 0.1 M ammonium acetate in 80% methanol. Proteins were then

solubilized in 50 mM ammonium bicarbonate for a reduction-alkylation step (dithiothreitol 5 mM – iodoacetamide 10 mM) and an overnight digestion with 300ng of sequencing-grade porcine trypsin (Promega, Fitchburg, MA, USA). Digested peptides were resuspended in 0.1% formic acid (solvent A) and injected on an Easy-nanoLC-1000 system coupled to a Q-Exactive Plus mass spectrometer (Thermo Fisher Scientific, Germany). One fourth of each sample was loaded on a C-18 precolumn (75 µm ID × 20 mm nanoViper, 3µm Acclaim PepMap; Thermo-Fisher Scientific) and separated on an analytical C18 analytical column (75 µm ID × 25 cm nanoViper, 3µm Acclaim PepMap) with a 160 minutes gradient of solvent B (0.1% of formic acid in acetonitrile).

Qexactive data were searched with Mascot algorithm (version 2.6.2, Matrix Science) against the Swissprot database with *H.sapiens* taxonomy (release 2020_05) as well as the sequences of GFP and of SINV virus (20 394 sequences) with a decoy strategy. The resulting .dat Mascot files were then imported into Proline v2.0 software (Bouyssié et al., 2020) to align the identified proteins. Proteins were then validated on Mascot pretty rank equal to 1, 1% FDR on both peptide spectrum matches (PSM) and protein sets (based on Mascot score).

For statistical analyses of the mass spectrometry data, spectral counts (SpC) of the identified proteins were stored in a local MongoDB database and subsequently analysed through a Shiny Application built upon the R packages msmsEDA (Gregori J, Sanchez A, Villanueva J (2014). msmsEDA: Exploratory Data Analysis of LC-MS/MS data by spectral counts. R/Bioconductor package version 1.22.0) and msmsTests (Gregori J, Sanchez A, Villanueva J (2013). msmsTests: LC-MS/MS Differential Expression Tests. R/Bioconductor package version 1.22.0). Differential expression tests were performed using a negative binomial regression model. The P-values were adjusted with FDR control by the Benjamini–Hochberg method and the following criteria were used to define differentially expressed proteins: an adjusted P-value <0.05, a minimum of 5 SpC in the most abundant condition, and a minimum absolute Log2 fold change of 1.

2.14. Data deposition

The mass spectrometry proteomics data have been deposited to the ProteomeXchange Consortium via the PRIDE (Perez-Riverol et al., 2022) partner repository with the dataset identifier PXD044867 and 10.6019/PXD044867.

3. Results

3.1. DDX5 depletion reduces SINV infection in HCT116 cells.

To formally determine the impact of DDX5 on SINV replication and infection, we first knocked it down by siRNA treatment in HCT116 cells, which were then infected for 24h with SINV-GFP at an MOI of 0.1. We observed a reduction in viral capsid protein level by western blot (**Figure S1A**) and a decrease in GFP expression by fluorescent microscopy (**Figure S1B**) upon DDX5 depletion (siDDX5) compared to the control condition (siCTRL). In addition, we found that the viral genomic (g)RNA level (**Figure S1C**) and the viral titer (**Figure S1D**) were also reduced in siDDX5 compared to siCTRL-treated cells.

To further establish the negative effect of DDX5 depletion on SINV infection, we generated homozygous *DDX5* knockout (KO) HCT116 cells by CRISPR/Cas9 (**Figure 1A**). The *DDX5* KO clone was characterized at the genomic DNA level (**Figure 1A-B**) and the absence of DDX5 protein was verified by western blot (**Figure 1C**).

Upon SINV-GFP infection for 24h at an MOI of 0.1 we observed a strong reduction in viral capsid protein in *DDX5* KO HCT116 compared to WT HCT116 cells by western blot (**Figure 1C**). The viral genomic RNA level (**Figure 1D**) and the viral titer (**Figure 1E**) were also significantly reduced in the absence of DDX5.

We also used the relative fluorescence of GFP to quantify the impact of *DDX5* knockout during a time course of SINV infection using a CellcyteX automated cell counter and analyser. A robust decrease in GFP fluorescence signal was observed in SINV-GFP infected *DDX5* KO compared to WT HCT116 cells at the three MOIs tested (MOI of 0.01, 0.1 and 1) over 72 hours (**Figure 1F**). These results indicate that DDX5 depletion strongly reduces the infection over time and independently on the MOI used already at the earliest step of the viral replication cycle. Taken together our results point to a negative impact of DDX5 depletion on SINV infection in our experimental conditions suggesting that DDX5 is a pro-viral host factor for SINV infection.

3.2. DDX5 interacts with SINV viral RNA in the cytoplasm of SINV -infected cells.

It was previously reported that DDX5 is primarily localized in the nucleus (Xing et al., 2019), while the SINV replication cycle is strictly cytoplasmic (Griffin, 2007).

To determine whether the observed effect of DDX5 on SINV infection depends on a direct interaction between DDX5 and viral components, for instance the viral RNA, we first verified

whether DDX5 co-localizes with SINV RNA in infected cells. Despite the predominantly nuclear localization in uninfected cells, confocal microscopy analyses showed that DDX5 re-localizes to the cytoplasm in the presence of the virus and co-localizes with the viral genomic RNA at 24 hours post infection (**Figure 2A**). We subsequently performed RNA immunoprecipitation (RIP) on the endogenous DDX5 in mock and SINV GFP-infected HCT116 cells. Efficient DDX5 immunoprecipitation was assessed at the protein level by western blot (**Figure S2A)** and the associated RNA was analysed**.**

We then found that the viral genomic RNA is specifically enriched in the DDX5-RIP compared to the control (IgG-RIP) condition by RT-qPCR (**Figure 2B**). We also performed dot blot analyses using a J2 antibody which detects dsRNA longer than 40 bp (Bonin et al., 2000; Schonborn et al., 1991) and observed an enrichment of dsRNAs in the DDX5-IP compared to the IgG-IP upon SINV infection (**Figure 2C**). Of particular note, we also observed enrichment of dsRNA in the mock condition, albeit to a lesser degree than upon SINV infection. This suggests that DDX5 binds to endogenous dsRNA molecules even in the absence of viral RNA. Whilst dsRNA can be found associated with DDX5 by dot blot analyses, confocal co-immunostaining analyses using the J2 as a proxy for dsRNA do not demonstrate a clear co-localization of DDX5 and dsRNA upon SINV-infection (**Figure S2B**), but rather indicate a proximity between the protein and dsRNA.

Overall, these results suggest that DDX5 can bind to viral RNA in the cytoplasm of SINV infected cells and localizes in close proximity to cytoplasmic viral RNA structures.

3.3. DDX5 interacts with the viral capsid in SINV infected cells.

Once we determined that DDX5 could associate with viral RNA, we asked whether any interaction between DDX5 and any of the viral proteins could also occur. We chose to test all four SINV non-structural proteins (nsP1, nsP2, nsP3, nsP4) required for viral RNA synthesis and the structural capsid protein (CP) which associates with the viral genomic RNA for its packaging (**Figure 3A**). We individually cloned each of their coding sequence in order to express them with an N-terminal Flag-HA tag and verified their expression upon transient transfection in HCT116 cells by western blot analysis using an anti-Flag antibody (**Figure S3**). We next investigated whether the endogenous DDX5 co-immunoprecipitated with any of the overexpressed viral proteins in uninfected HCT116 cells in the absence of viral RNA or any other viral protein. We observed that the capsid protein interacted with DDX5 suggesting that such an interaction could be direct (**Figure 3B**).

We then performed co-immunostaining analyses to verify whether DDX5 co-localizes with the viral capsid in SINV-infected HCT116 cells. Confocal microscopy analysis demonstrated that endogenous DDX5 partially co-localizes with the capsid protein in SINV infected cells indicating the possibility that the two proteins interact upon infection (**Figure 3C**).

3.4. DDX5 interacts with DDX17 and capsid in SINV-infected conditions.

To better understand how DDX5 could act as a pro-viral factor upon SINV infection we decided to characterize its interactome in mock and SINV-infected HCT116 cells. We immunoprecipitated DDX5 in uninfected and SINV-GFP infected HCT116 cells at MOI 0.1 for 24 hours with a rabbit anti-DDX5 antibody and eluates were analysed by liquid chromatography coupled to tandem mass spectrometry (LC-MS/MS). A rabbit IgG antibody was used as a negative control. Significantly enriched proteins were determined as having an FDR<1%, at least 5 spectral counts in the most abundant condition, a fold change of at least 2 and an adjusted p-value lower than 0.05.

Differential expression analysis revealed a total of 206 human proteins enriched in uninfected DDX5-IP over mock IgG-IP conditions (**Figure S4A** and **Table 1**), while 175 human and 2 viral proteins were enriched in DDX5 IP over IgG IP control in SINV-infected samples (**Figure 4A and Table 2**). Viral capsid and nsP2 were the top hits among the significantly enriched proteins in DDX5 IP SINV over DDX5 IP mock (**Figure S4B** and **Table 3**). Therefore, the proteomics results confirmed the interaction between the viral capsid and DDX5 in infected cells that we previously observed by immunofluorescence (**Figure 3**) and revealed that nsP2 could also associate with DDX5 in the presence of the virus.

Comparison of the DDX5 enrichment profiles in SINV (**Figure 4A** and **Table 2**) and mock (**Figure S4A** and **Table 1**) conditions showed that only 21 proteins were found to be enriched in DDX5 IP over IgG IP in infected conditions. Of note, 156 human proteins overlapped in the mock and SINV DDX5 interactomes, suggesting an overall stable DDX5 interactome core before and after infection (**Figure S4C**). Among them, we identified several RNA helicases such as DHX9, DHX30, DHX15, DDX3X, DDX21, DDX24, DDX54, DDX18, DDX10, DDX52 and DDX56. In particular, one of the most enriched human proteins in both mock and SINV- infected DDX5 IP was its well-known interactor DDX17 (Ogilvie et al., 2003). Another interesting factor associated with DDX5 in both uninfected and infected conditions was the polyribonucleotide nucleotidyltransferase 1 (PNPT1).

This enzyme is predominantly localized in the mitochondrial intermembrane space and acts as a 3'-to-5' exoribonuclease to regulate mitochondrial RNA metabolism thereby modulating innate immunity (Dhir et al., 2018). To our knowledge, the interaction between human PNPT1 and DDX5 has not been reported so far.

We further validated the interaction of DDX5 with DDX17 and the viral capsid upon SINV infection by co-immunoprecipitation experiments (**Figure 4B**). In addition, reciprocal co-immunoprecipitation of DDX17 confirmed its interaction with DDX5 and the viral capsid, suggesting that the three proteins may belong to the same complex (**Figure 4C**). These observations were supported by co-immunostaining using combinations of specific antibodies for DDX5 and DDX17 (**Figure 4D**). Interestingly, while DDX17 and DDX5 colocalize in the nucleus in uninfected conditions, both proteins re-localize to the cytoplasm in discrete perinuclear foci upon SINV infection (**Figure 4D)** in proximity of viral replication sites (see **Figure 2A**).

3.5.Combined DDX5 and DDX17 depletion has a cumulative detrimental impact on SINV.

To determine whether DDX17 plays a role during SINV infection independently of or together with DDX5, we first knocked down DDX17 then infected HCT116 cells with SINV-GFP. We validated the knockdown efficiency by western blot compared to an siRNA control and observed that viral capsid levels were reduced upon siDDX17 treatment (**Figure 5A**). In addition, SINV genomic and sub-genomic RNA levels (**Figure 5B-C**) as well as SINV viral particle production (**Figure 5D**) were also significantly reduced in DDX17 knockdown conditions compared to siCTRL. These results suggested that just like DDX5, DDX17 is a proviral factor for SINV infection.

We proceeded to investigate whether DDX17 acts in synergy or competition with DDX5 by analysing the impact of DDX17 knockdown in *DDX5* KO HCT116 cells where viral infection is already weakened (**Figure 1C and S5**). As previously reported (Jalal et al., 2007), we first observed that protein levels of both DDX7 isoforms (p72 and p82) increased in *DDX5* KO HCT116 compared to WT HCT116 cells and that such an effect was independent on the infection (**Figure S5**). We then confirmed the efficiency of DDX17 knockdown in SINV GFP-infected *DDX5* KO HCT116 cells by western blot and we observed a further reduction of the viral capsid expression upon siDDX17 treatment compared to the control condition (**Figure 6A**). SINV genomic and sub-genomic RNA levels (**Figure 6B-C**) as well as SINV viral particle production (**Figure 6D**) were significantly diminished in DDX17 knockdown conditions

compared to siCTRL in *DDX5* KO HCT116 cells. Overall, these results indicate that DDX5 and DDX17 may have independent pro-viral functions during SINV infection because their individual depletion causes reduction of viral infection at the protein, RNA and viral production levels and their joint depletion has a cumulative negative effect on SINV infection.

4. Discussion

The human DEAD-box RNA helicase DDX5 plays a pivotal role in virus–host interaction being mostly pro-viral for several viral families. In this study, we investigated and extended the function of DDX5 as a cellular cofactor of SINV replication.

We found that DDX5 interacts with viral RNA at the cytoplasmic viral replication sites, which may be important for its pro-viral activity. RNA helicases recognize the RNA structure rather than their sequence and they have shown little substrate specificity *in vitro* (Tanner and Linder, 2001). This lack of specificity is counterbalanced by their association with specific interactors *in vivo*. For instance, DDX5 interaction with either viral non-structural or structural proteins is essential for its pro-viral role across different RNA virus infections (Cheng et al., 2018).

Our proteomic results, supported by co-immunoprecipitation experiments and imaging analyses, revealed the interaction between DDX5 and SINV capsid, as well as with the nsP2 protein. The cytoplasmic SINV capsid protein is essential for genomic RNA packaging and the first steps of viral morphogenesis. In contrast, SINV nsP2 is the protease and helicase of the viral replication complex and it is the only viral protein known to re-localise to the nucleus to inhibit host transcription (Akhrymuk et al., 2012). The interaction between DDX5 and nsP2 may thus occur both in the nucleus and in the cytoplasm of the infected cell. Whether the association with the viral proteins is RNA-dependent and if it is necessary for DDX5 binding to the viral RNA also remains to be established.

The DDX5 interactome analysis also revealed interactions with a number of cellular RNA binding proteins that could have a function during SINV infection. These include several RNA helicases of the DEAD/H family and other interesting factors such as PNPT1. Interestingly, we previously showed that DDX5, DDX17 and PNPT1 are an integral part of the SINV dsRNA associated proteome (Girardi et al., 2023). In this study we focused on DDX17 which was previously known to associate with DDX5. Further investigations are needed to better characterize if the association of other novel interactors with DDX5 have functional consequences on SINV infection.

It is now established that the replication of positive strand RNA viruses in the cytoplasm can induce re-localization of nuclear host proteins and promote infection (Lloyd, 2015). Of note,

DDX5 re-localizes from the nucleus to the cytoplasm with DDX17 upon SINV infection and they both interact with the viral capsid protein. It is thus conceivable that DDX17 operates with DDX5 within the same complex, carrying out a cumulative function during infection.

A previous study showed that Rm62, the fly orthologue of DDX17 and DDX5, did not affect SINV infection in *D. melanogaster*, and that DDX17 knockdown showed no antiviral effect on the accumulation of SINV capsid protein in human U2OS cells (Moy et al., 2014). In contrast, we demonstrated that single depletion of DDX17 reduces SINV infection in HCT116 cells and its combined depletion with DDX5 in the KO background further decreases viral levels, suggesting a synergism between the two proteins in promoting viral infection.
These experiments ruled out the possibility that the observed reduction in SINV replication upon DDX5 depletion was due to an antiviral effect of compensatory DDX17 overexpression.

We showed that DDX5 depletion has a detrimental effect on viral replication and production in infected HCT116 cells. Despite being an uncommon model to study alphavirus infection, the HCT116 cell line was chosen because it can be easily infected with SINV and can be used for CRISPR-Cas9 gene editing procedures (Petitjean et al., 2020). It will, however, be important to expand our functional observations to other cellular models more relevant for alphavirus infection in the future.

As both DDX5 and DDX17 inhibition reduces virus levels, further investigation is required to better characterize these factors as potential targets for antiviral therapies.
Additional analyses will be needed to formally assess whether DDX5 direct action supports viral replication and if its binding to viral RNA and helicase activity is necessary for its function. Being involved in many aspects of cellular RNA biology, one cannot formally exclude the contribution of DDX5 indirect effects on infection. For instance, DDX5 activity as a regulator of N6-methyladenosine levels on the DHX58 and NFκB mRNAs could negatively impact antiviral innate immunity and therefore enhance viral infection (Xu et al., 2021). Finally, it could be of interest to determine whether the helicase activity of DDX5 or DDX17 is required for their cumulative pro-viral effect on SINV production and which protein domains are important for their interaction with capsid or nsP2 viral proteins.

5. Conclusion

In conclusion, this study significantly advances our understanding of the crucial role played by DDX5 and DDX17 as host positive factors in viral infections and uncovers their function on the prototype alphavirus SINV. Our results demonstrate the interaction of DDX5 with viral RNA, suggesting a potential impact on early stages of viral replication. We discovered a re-localization of DDX5 together with its partner DDX17 to the cytoplasm upon SINV infection and their association with the viral capsid protein. Of note, depletion of both DDX5 and DDX17 strongly impacts SINV infection. Even if the exact mechanism of action warrants further investigation, DDX5 and DDX17 may hold promise as targets for future antiviral therapies.

Figure legends

Figure 1: SINV infection in WT and CRISPR/Cas9 *DDX5* knockout HCT116 cells. A) Schematic diagram of the *DDX5* CRIPR/Cas9 KO strategy. Two gRNAs targeting *DDX5* exon 2 and intron 2 respectively were used to delete the 5' splice site (ss) region (5'ss is shown in green, #1 target region in blue and #2 target region in magenta). The purple arrow represents an indel in *DDX5* exon 2 for the KO allele 1. The grey rectangle represents a 378 nucleotide (nt) deletion in KO allele 2. **B**) Agarose gel showing the PCR fragments amplified from cellular genomic DNA, corresponding to the WT and KO alleles, respectively, which were gel purified and sequenced. Amplicon size is shown: the upper band corresponds to KO allele 1, the lower band corresponds to the KO allele 2. **C)** Western blot on mock or SINV-GFP infected cells in WT or *DDX5* KO HCT116 cells. Antibodies against DDX5 and viral capsid were used. GAPDH was used as loading normalizer. **D**) Level of SINV genomic RNA relative to GAPDH monitored by RT-qPCR in WT or *DDX5* KO HCT116 cells upon SINV-GFP infection at MOI 0.1 for 24 hours. Results are plotted as fold change relative to WT cells. **E**) Viral particles of SINV-GFP from the supernatant of SINV-GFP infected WT or *DDX5* KO HCT116 cells were quantified by plaque assay on Vero cells by plaque assay. The results from three independent experiments are presented here. **F**) SINV-GFP infection kinetics in WT and *DDX5* KO HCT116 cells. The relative GFP fluorescence area (expressed as percentage of the total area) of WT and *DDX5* KO HCT116 cells as a function of time was measured after SINV GFP infection at an MOI of 0.01 (left panel), 0.1 (middle panel) and 1 (right panel) every 6 hours for 72 hours with a CellcyteX automated cell counter and analyser. WT HCT116 cells, black; *DDX5* KO HCT116 cells, red. Error bars in **D-E** and **F** represent the mean ± standard deviation (SD) of three independent biological experiments. * $p \leq 0.05$, ** $p \leq 0.01$, (**D**) one- sample t test or (**E**) paired Student's t test.

Figure 2: DDX5 interacts with the viral RNA. A) Confocal microscopy analysis of SINV (+) RNA and DDX5 protein localization in mock and infected HCT116 cells at 24 hpi by RNA fluorescence in situ hybridization (FISH) (in magenta) combined with protein immunostaining (in green). DAPI staining (in blue) and merge of the different channels are shown. Magnification 40X, scale bar, 10µm. **B**) RT-qPCR on SINV genomic (g) RNA upon DDX5 RIP or IgG RIP. Results are expressed as percentage of Input (total RNA) and represent the mean ± standard deviation (SD) of three biological replicates (n = 3). **C**) Anti-dsRNA dot blot

assay on serial dilutions of the total RNA (INPUT) and the undiluted RNA samples from DDX5-RIP or IgG-RIP, in mock and SINV infected conditions. J2 antibody was used to detect dsRNAs.

Figure 3: DDX5 interacts with the SINV capsid protein. A) Schematic illustration of SINV genomic organization. The 5´ cap and poly(A) tail are depicted. The non-structural proteins (np1, nsp2, nsp3, nsp4) from the first ORF (in green) and the structural proteins (capsid, E3, E2, 6K, E1) from the second ORF (in yellow and grey) are shown. The nucleotides (nt) corresponding to the beginning and the end of viral sequences cloned to individually overexpress the nsp1, nsP2, nsP3, nsP4 and capsid proteins with an N-terminally FLAG-HA tag are indicated. **B**) Western blot on total lysate (INP) or anti-HA IP (IP) from transiently transfected HCT116 cells using anti-FLAG and anti-DDX5 antibodies. Position and molecular weight (KDa) of protein size markers are shown on the left. **C**) Confocal co-immunofluorescence analysis performed in mock and SINV- infected HCT116 cells using anti-capsid (in green) or anti-DDX5 antibody (in magenta) is shown. DAPI was used to stain the nuclei (in blue). Magnifications 40X, scale bar 10µm.

Figure 4: DDX5 interactome in mock and SINV-infected cells. A) Volcano plot showing the global protein enrichment in SINV-DDX5-IP versus SINV-IgG-IP using data from three independent replicates. The cells were infected with SINV-GFP during for 24h at an MOI 0.1. Significantly enriched or depleted proteins are represented in red or blue, respectively. Cut off values: FDR<1%, at least 5 spectral counts in the most abundant condition, fold change > 2, adjusted p-value lower than 0.05. Viral proteins and selected host proteins are circled in black and orange, respectively. **B**) Western blot on total lysate (INPUT), IgG-IP (IgG) or DDX5-IP (DDX5) samples in both mock and SINV-GFP infected HCT116 cells using antibodies against DDX5, DDX17 and viral capsid. **C**) Western blot on total lysate (INPUT), IgG-IP (IgG) or DDX17-IP (DDX17) samples in both mock and SINV-GFP infected HCT116 cells using antibodies against DDX17, DDX5 and viral capsid. **D**) Confocal co-immunofluorescence analysis is performed on mock and SINV-infected HCT116 cells using (**D**) rabbit anti-DDX5 and mouse anti-DDX17 primary antibodies, coupled to secondary anti rabbit (in green) or anti-mouse (in magenta) antibodies. DAPI was used to stain the nuclei (in blue). Magnifications 40X, scale bar 10µm.

Figure 5: Effect of DDX17 depletion on SINV in HCT116 cells. A) Western blot on SINV-GFP infected HCT116 cells, treated with siCTRL and siDDX17. Antibodies directed against DDX5, DDX17 and capsid were used. Tubulin antibody was used as loading control. (**B-C**) RT-qPCR of SINV genomic (g) RNA (**B**) and SINV sub-genomic (sg) RNA (**C**) in siRNA treated SINV-GFP infected HCT116 cells (MOI 0.1, 24 hpi). Results are expressed as relative to GAPDH and normalized over the siCTRL condition. **D**) SINV-GFP viral titers from infected HCT116 cells transfected with the indicated siRNAs, quantified by plaque assay. Results in (**B-C- D)** represent the mean ± standard deviation of three biological replicates (n = 3). * $p \leq 0.05$, (**B-C**) one sample t test or (**D**) paired Student's t test.

Figure 6: Effect of DDX17 depletion on SINV in *DDX5* KO HCT116 cells. A) Western blot of samples from SINV-GFP infected *DDX5* KO HCT116 cells upon siCTRL or siDDX17 transfection. Specific primary antibodies against DDX5, DDX17 and viral capsid were used. Tubulin was used as loading control. Position and molecular weight (KDa) of protein size markers are shown on the left. **B-C)** RT-qPCR of SINV genomic (g) RNA (**B**) and SINV sub-genomic (sg) RNA (**C**) in SINV-GFP infected *DDX5* KO HCT116 cells (MOI 0.1, 24 hpi), upon siRNA transfection. **D)** SINV-GFP viral titers from infected *DDX5* KO HCT116 cells transfected with the indicated siRNAs, quantified by plaque assay. Results are expressed as relative to GAPDH and normalized to the siCTRL condition. Results in **B-C-D** represent the mean ± standard deviation of three biological replicates (n = 3). * $p \leq 0.05$, **$p \leq 0.01$, (**B-C**) one- sample t test or (**D**) paired Student's t test.

Acknowledgements

We thank Béatrice Chane-Woon-Ming for her help with the proteomic analyses and Dr. Paula Lopez for her initial support with plaque assays. We also thank Dr. Carla Saleh for providing the SINV WT and GFP infectious clones and Dr. Diane Griffin for providing the CAPSID antibody. We thank Dr. Cyril Bourgeois, Dr. Patryk Ngondo and members of the Pfeffer labs for critical reading of the manuscript. This work received financial support from the Agence Nationale de la Recherche (EndoDRAI project ANR-22-CE15-0011-01 (to E.G.) and was supported by the Idex 2022 Attractivité grant under the framework of the IdeX University of Strasbourg (to E.G.) and from the French Minister for Higher Education, Research and Innovation (PhD contract to C.P.). This work of the Interdisciplinary Thematic Institute IMCbio+, as part of the ITI 2021-2028 program of the University of Strasbourg, CNRS and Inserm, was supported by IdEx Unistra (ANR-10-IDEX-0002), by SFRI-STRAT'US project (ANR-20-SFRI-0012), EUR IMCBio (IMCBio ANR-17-EURE-0023) under the framework of the French Investments for the Future Program. S.P. also receive funding from ANR (Project RIFLAVIRAM ANR-21-CE35-0018-01). The mass spectrometry instrumentations were funded by the University of Strasbourg, IdEx "Equipement mi-lourd" 2015.

CRediT authorship contribution statement

Mélanie Messmer: Conceptualization, Methodology, Validation, Investigation, Visualization, Writing - Original Draft. **Louison Pierson**: Investigation. **Charline Pasquier**: Investigation. **Nikola Djordjevic**: Investigation. **Johana Chicher**: Investigation, Validation. **Philippe Hammann**: Investigation, Validation. **Sébastien Pfeffer**: Conceptualization., Writing - Review & Editing, Funding acquisition. **Erika Girardi**: Conceptualization, Methodology, Validation, Investigation, Visualization, Writing - Review & Editing, Funding acquisition, Supervision.

References

Akhrymuk, I., Kulemzin, S.V., Frolova, E.I., 2012. Evasion of the Innate Immune Response: the Old World Alphavirus nsP2 Protein Induces Rapid Degradation of Rpb1, a Catalytic Subunit of RNA Polymerase II. J Virol 86, 7180–7191. https://doi.org/10.1128/JVI.00541-12

Bonaventure, B., Goujon, C., 2022. DExH/D-box helicases at the frontline of intrinsic and innate immunity against viral infections. Journal of General Virology 103. https://doi.org/10.1099/jgv.0.001766

Bonin, M., Oberstraß, J., Lukacs, N., Ewert, K., Oesterschulze, E., Kassing, R., Nellen, W., 2000. Determination of preferential binding sites for anti-dsRNA antibodies on double-stranded RNA by scanning force microscopy. RNA 6, 563–570. https://doi.org/10.1017/S1355838200992318

Bouyssié, D., Hesse, A.-M., Mouton-Barbosa, E., Rompais, M., Macron, C., Carapito, C., de Peredo, A.G., Couté, Y., Dupierris, V., Burel, A., Menetrey, J.-P., Kalaitzakis, A., Poisat, J., Romdhani, A., Burlet-Schiltz, O., Cianférani, S., Garin, J., Bruley, C., 2020. Proline: an efficient and user-friendly software suite for large-scale proteomics. Bioinformatics. https://doi.org/10.1093/bioinformatics/btaa118

Chen, J.-Y., Chen, W.-N., Poon, K.-M.V., Zheng, B.-J., Lin, X., Wang, Y.-X., Wen, Y.-M., 2009. Interaction between SARS-CoV helicase and a multifunctional cellular protein (Ddx5) revealed by yeast and mammalian cell two-hybrid systems. Arch Virol 154, 507–512. https://doi.org/10.1007/s00705-009-0323-y

Cheng, W., Chen, G., Jia, H., He, X., Jing, Z., 2018. DDX5 RNA Helicases: Emerging Roles in Viral Infection. IJMS 19, 1122. https://doi.org/10.3390/ijms19041122

Dardenne, E., Polay Espinoza, M., Fattet, L., Germann, S., Lambert, M.-P., Neil, H., Zonta, E., Mortada, H., Gratadou, L., Deygas, M., Chakrama, F.Z., Samaan, S., Desmet, F.-O., Tranchevent, L.-C., Dutertre, M., Rimokh, R., Bourgeois, C.F., Auboeuf, D., 2014. RNA Helicases DDX5 and DDX17 Dynamically Orchestrate Transcription, miRNA, and Splicing Programs in Cell Differentiation. Cell Reports 7, 1900–1913. https://doi.org/10.1016/j.celrep.2014.05.010

Dhir, A., Dhir, S., Borowski, L.S., Jimenez, L., Teitell, M., Rötig, A., Crow, Y.J., Rice, G.I., Duffy, D., Tamby, C., Nojima, T., Munnich, A., Schiff, M., De Almeida, C.R., Rehwinkel, J., Dziembowski, A., Szczesny, R.J., Proudfoot, N.J., 2018. Mitochondrial double-stranded RNA triggers antiviral signalling in humans. Nature 560, 238–242. https://doi.org/10.1038/s41586-018-0363-0

Girardi, E., Messmer, M., Lopez, P., Fender, A., Chicher, J., Chane-Woon-Ming, B., Hammann, P., Pfeffer, S., 2023. Proteomics-based determination of double-stranded RNA interactome reveals known and new factors involved in Sindbis virus infection. RNA 29, 361–375. https://doi.org/10.1261/rna.079270.122

Goh, P.-Y., Tan, Y.-J., Lim, S.P., Tan, Y.H., Lim, S.G., Fuller-Pace, F., Hong, W., 2004. Cellular RNA Helicase p68 Relocalization and Interaction with the Hepatitis C Virus (HCV) NS5B Protein and the Potential Role of p68 in HCV RNA Replication. J Virol 78, 5288–5298. https://doi.org/10.1128/JVI.78.10.5288-5298.2004

Griffin, D., 2007. Alphaviruses, p 1023–1067, in: Fields Virology, 5th Ed. Lippincott Williams & Wilkins, Philadelphia, PA.

Hu, M., Zheng, H., Wu, J., Sun, Y., Wang, T., Chen, S., 2022. DDX5: an expectable treater for viral infection- a literature review. Ann Transl Med 10, 712–712. https://doi.org/10.21037/atm-22-2375

Jalal, C., Uhlmann-Schiffler, H., Stahl, H., 2007. Redundant role of DEAD box proteins p68 (Ddx5) and p72/p82 (Ddx17) in ribosome biogenesis and cell proliferation. Nucleic Acids Research 35, 3590–3601. https://doi.org/10.1093/nar/gkm058

Janknecht, R., 2010. Multi-talented DEAD-box proteins and potential tumor promoters: p68 RNA helicase (DDX5) and its paralog, p72 RNA helicase (DDX17). Am J Transl Res 2, 223–234.

Li, C., Ge, L., Li, P., Wang, Y., Sun, M., Huang, L., Ishag, H., Di, D., Shen, Z., Fan, W., Mao, X., 2013. The DEAD-box RNA helicase DDX5 acts as a positive regulator of Japanese encephalitis virus replication by binding to viral 3′ UTR. Antiviral Research 100, 487–499. https://doi.org/10.1016/j.antiviral.2013.09.002

Lin, C., Yang, L., Yang, J.J., Huang, Y., Liu, Z.-R., 2005. ATPase/Helicase Activities of p68 RNA Helicase Are Required for Pre-mRNA Splicing but Not for Assembly of the Spliceosome. Molecular and Cellular Biology 25, 7484–7493. https://doi.org/10.1128/MCB.25.17.7484-7493.2005

Linder, P., Jankowsky, E., 2011. From unwinding to clamping — the DEAD box RNA helicase family. Nat Rev Mol Cell Biol 12, 505–516. https://doi.org/10.1038/nrm3154

Liu, Z.-R., 2002. p68 RNA Helicase Is an Essential Human Splicing Factor That Acts at the U1 snRNA-5′ Splice Site Duplex. Molecular and Cellular Biology 22, 5443–5450. https://doi.org/10.1128/MCB.22.15.5443-5450.2002

Lloyd, R.E., 2015. Nuclear proteins hijacked by mammalian cytoplasmic plus strand RNA viruses. Virology 479–480, 457–474. https://doi.org/10.1016/j.virol.2015.03.001

López, P., Girardi, E., Mounce, B.C., Weiss, A., Chane-Woon-Ming, B., Messmer, M., Kaukinen, P., Kopp, A., Bortolamiol-Becet, D., Fendri, A., Vignuzzi, M., Brino, L., Pfeffer, S., 2020. High-Throughput Fluorescence-Based Screen Identifies the Neuronal MicroRNA miR-124 as a Positive Regulator of Alphavirus Infection. J Virol 94, e02145-19, /jvi/94/9/JVI.02145-19.atom. https://doi.org/10.1128/JVI.02145-19

Meier-Stephenson, V., Mrozowich, T., Pham, M., Patel, T.R., 2018. DEAD-box helicases: the Yin and Yang roles in viral infections. Biotechnology and Genetic Engineering Reviews 34, 3–32. https://doi.org/10.1080/02648725.2018.1467146

Montavon, T.C., Baldaccini, M., Lefèvre, M., Girardi, E., Chane-Woon-Ming, B., Messmer, M., Hammann, P., Chicher, J., Pfeffer, S., 2021. Human DICER helicase domain recruits PKR and modulates its antiviral activity. PLoS Pathog 17, e1009549. https://doi.org/10.1371/journal.ppat.1009549

Moy, R.H., Cole, B.S., Yasunaga, A., Gold, B., Shankarling, G., Varble, A., Molleston, J.M., tenOever, B.R., Lynch, K.W., Cherry, S., 2014. Stem-Loop Recognition by DDX17 Facilitates miRNA Processing and Antiviral Defense. Cell 158, 764–777. https://doi.org/10.1016/j.cell.2014.06.023

Ogilvie, V.C., Wilson, B.J., Nicol, S.M., Morrice, N.A., Saunders, L.R., Barber, G.N., Fuller-Pace, F.V., 2003. The highly related DEAD box RNA helicases p68 and p72 exist as heterodimers in cells. Nucleic Acids Res 31, 1470–1480.

Perez-Riverol, Y., Bai, J., Bandla, C., García-Seisdedos, D., Hewapathirana, S., Kamatchinathan, S., Kundu, D.J., Prakash, A., Frericks-Zipper, A., Eisenacher, M., Walzer, M., Wang, S., Brazma, A., Vizcaíno, J.A., 2022. The PRIDE database resources in 2022: a hub for mass spectrometry-based proteomics evidences. Nucleic Acids Research 50, D543–D552. https://doi.org/10.1093/nar/gkab1038

Petitjean, O., Girardi, E., Ngondo, R.P., Lupashin, V., Pfeffer, S., 2020. Genome-Wide CRISPR-Cas9 Screen Reveals the Importance of the Heparan Sulfate Pathway and the Conserved Oligomeric Golgi Complex for Synthetic Double-Stranded RNA Uptake and Sindbis Virus Infection. mSphere 5, e00914-20. https://doi.org/10.1128/mSphere.00914-20

Rahman, M.M., Bagdassarian, E., Ali, M.A.M., McFadden, G., 2017. Identification of host DEAD-box RNA helicases that regulate cellular tropism of oncolytic Myxoma virus in human cancer cells. Sci Rep 7, 15710. https://doi.org/10.1038/s41598-017-15941-1

Ran, F.A., Hsu, P.D., Wright, J., Agarwala, V., Scott, D.A., Zhang, F., 2013. Genome engineering using the CRISPR-Cas9 system. Nat Protoc 8, 2281–2308. https://doi.org/10.1038/nprot.2013.143

Ríos-Marco, P., Romero-López, C., Berzal-Herranz, A., 2016. The cis-acting replication element of the Hepatitis C virus genome recruits host factors that influence viral replication and translation. Sci Rep 6, 25729. https://doi.org/10.1038/srep25729

Schonborn, J., Oberstraβ, J., Breyel, E., Tittgen, J., Schumacher, J., Lukacs, N., 1991. Monoclonal antibodies to double-stranded RNA as probes of RNA structure in crude nucleic acid extracts. Nucl Acids Res 19, 2993–3000. https://doi.org/10.1093/nar/19.11.2993

Sithole, N., Williams, C.A., Abbink, T.E.M., Lever, A.M.L., 2020. DDX5 potentiates HIV-1 transcription as a co-factor of Tat. Retrovirology 17, 6. https://doi.org/10.1186/s12977-020-00514-4

Tanner, N.K., Linder, P., 2001. DExD/H Box RNA Helicases. Molecular Cell 8, 251–262. https://doi.org/10.1016/S1097-2765(01)00329-X

Taschuk, F., Cherry, S., 2020. DEAD-Box Helicases: Sensors, Regulators, and Effectors for Antiviral Defense. Viruses 12, 181. https://doi.org/10.3390/v12020181

Weaver, S.C., Barrett, A.D.T., 2004. Transmission cycles, host range, evolution and emergence of arboviral disease. Nat Rev Microbiol 2, 789–801. https://doi.org/10.1038/nrmicro1006

Xing, Z., Ma, W.K., Tran, E.J., 2019. The DDX5/Dbp2 subfamily of DEAD-box RNA helicases. WIREs RNA 10. https://doi.org/10.1002/wrna.1519

Xu, J., Cai, Y., Ma, Z., Jiang, B., Liu, W., Cheng, J., Guo, N., Wang, Z., Sealy, J.E., Song, C., Wang, X., Li, Y., 2021. The RNA helicase DDX5 promotes viral infection via regulating N6-methyladenosine levels on the DHX58 and NFκB transcripts to dampen antiviral innate immunity. PLoS Pathog 17, e1009530. https://doi.org/10.1371/journal.ppat.1009530

Zhang, H., Xing, Z., Mani, S.K.K., Bancel, B., Durantel, D., Zoulim, F., Tran, E.J., Merle, P., Andrisani, O., 2016. RNA helicase DEAD box protein 5 regulates Polycomb repressive complex 2/Hox transcript antisense intergenic RNA function in hepatitis B virus infection and hepatocarcinogenesis. Hepatology 64, 1033–1048. https://doi.org/10.1002/hep.28698

Zhao, S., Ge, X., Wang, X., Liu, A., Guo, X., Zhou, L., Yu, K., Yang, H., 2015. The DEAD-box RNA helicase 5 positively regulates the replication of porcine reproductive and respiratory syndrome virus by interacting with viral Nsp9 in vitro. Virus Research 195, 217–224. https://doi.org/10.1016/j.virusres.2014.10.021

Zhou, X., Luo, J., Mills, L., Wu, S., Pan, T., Geng, G., Zhang, J., Luo, H., Liu, C., Zhang, H., 2013. DDX5 Facilitates HIV-1 Replication as a Cellular Co-Factor of Rev. PLoS ONE 8, e65040. https://doi.org/10.1371/journal.pone.0065040

Tables

Table 1: List of significantly enriched proteins in mock-DDX5_IP versus mock-IgG_IP

1st column : Protein name
2nd column : Column named as the treatment level with the mean raw spectral counts observed for this condition
3rd column : Column named as the control level with the mean raw spectral counts observed for this condition

deltaSC : Difference between mean raw spectral counts
lFC.Av : Log fold change computed from the mean expression levels taking into account the given normalization factors.
logFC : Log fold change estimated by fitting the given GLM model. The reference level of the main factor is taken as control.

LR : The likelihood ratio for edgeR.

p.val : The unadjusted p-values obtained from the tests.

adjp : The multitest adjusted p-values with FDR control.

	mock_DDX5IP	mock_IgG_IP	deltaSC	lFC_Av	LogFC	LR	p_value	adjp	negLog_adjp
DDX5_HUMAN	745	0	745	Inf	11,8	164,9	9,65E-38	1,23E-34	33,91116
DDX21_HUMAN	136	0	136	Inf	9,338	70,22	5,31E-17	3,37E-14	13,47185
DDX17_HUMAN	109,7	0	109,7	Inf	9,036	52,04	5,44E-13	1,39E-10	9,85855
RL6_HUMAN	85,7	0,7	85	3,904	4,45	43,63	3,96E-11	6,30E-09	8,20087
YBOX1_HUMAN	120,3	2,3	118	3,687	3,213	43,71	3,80E-11	6,30E-09	8,20087
PABP1_HUMAN	74,3	0,7	73,6	5,681	4,273	39,23	3,76E-10	5,32E-08	7,27433
SRRM2_HUMAN	54,3	0	54,3	Inf	8,005	38,91	4,43E-10	5,63E-08	7,24934
PNPT1_HUMAN	81,3	0	81,3	Inf	8,602	37,99	7,11E-10	8,22E-08	7,08523
NOP56_HUMAN	47,7	0	47,7	Inf	7,821	36,84	1,29E-09	1,26E-07	6,90066
YBOX3_HUMAN	51,3	0	51,3	Inf	7,937	36,6	1,45E-09	1,32E-07	6,87976
RL35_HUMAN	49,7	0	49,7	Inf	7,883	35,93	2,05E-09	1,63E-07	6,78888
RS6_HUMAN	68,7	0,7	68	5,578	4,17	33,48	7,18E-09	5,11E-07	6,29183
RL4_HUMAN	182,3	7,7	174,6	2,104	2,056	33,47	7,23E-09	5,11E-07	6,29183
RL36_HUMAN	44	0	44	Inf	7,71	32,97	9,35E-09	6,26E-07	6,20336
RL13A_HUMAN	46,3	0	46,3	Inf	7,778	32,83	1,01E-08	6,40E-07	6,19389
SRRM1_HUMAN	42	0	42	Inf	7,65	30,17	3,96E-08	2,10E-06	5,67778
DHX9_HUMAN	65	0,7	64,3	5,5	4,095	30,24	3,83E-08	2,10E-06	5,67778

RL21_HUMAN	38,3	0	38,3	Inf	7,517	28,44	9,66E-08	4,91E-06	5,30865
RL1D1_HUMAN	40,7	0	40,7	Inf	7,606	28,02	1,20E-07	5,88E-06	5,23047
NAT10_HUMAN	34,7	0	34,7	Inf	7,369	27,6	1,49E-07	7,03E-06	5,15304
NOP2_HUMAN	36,7	0	36,7	Inf	7,457	27,52	1,56E-07	7,07E-06	5,15064
RL10A_HUMAN	65,3	1	64,3	4,928	3,555	27,36	1,69E-07	7,42E-06	5,12977
RL17_HUMAN	65,3	1,3	64	4,503	3,146	26,5	2,63E-07	1,12E-05	4,95273
DDX24_HUMAN	31,3	0	31,3	Inf	7,225	24,04	9,46E-07	3,20E-05	4,49444
HS90A_HUMAN	91,7	1,7	90	4,641	3,337	24,04	9,44E-07	3,20E-05	4,49444
TOP1_HUMAN	38,7	0,3	38,4	5,735	4,251	23,92	1,00E-06	3,27E-05	4,48545
KI67_HUMAN	53,3	0	53,3	Inf	7,98	23,63	1,17E-06	3,72E-05	4,42981
RL18A_HUMAN	52,3	1	51,3	4,597	3,222	23,42	1,30E-06	4,03E-05	4,39459
RS3_HUMAN	38	0,3	37,7	5,709	4,225	23,3	1,39E-06	4,11E-05	4,38669
RL27_HUMAN	30,7	0	30,7	Inf	7,197	22,9	1,71E-06	4,93E-05	4,30742
SRP72_HUMAN	27,7	0	27,7	Inf	7,04	22,24	2,41E-06	6,51E-05	4,18635
RLA2_HUMAN	36	0,3	35,7	5,643	4,154	21,95	2,81E-06	7,44E-05	4,12872
PABP4_HUMAN	42	0,7	41,3	4,858	3,453	21,83	2,97E-06	7,72E-05	4,11255
RS9_HUMAN	28,7	0	28,7	Inf	7,105	21,38	3,78E-06	9,11E-05	4,04072
RACK1_HUMAN	26,3	0	26,3	Inf	6,975	21,46	3,62E-06	9,11E-05	4,04072
RL18_HUMAN	75,3	2,3	73	3,002	2,534	21,38	3,78E-06	9,11E-05	4,04072
ILF3_HUMAN	27	0	27	Inf	7,013	21,28	3,97E-06	9,34E-05	4,0297
HNRL1_HUMAN	25	0	25	Inf	6,898	20,55	5,81E-06	0,0001319	3,87976
RRP1B_HUMAN	26,7	0	26,7	Inf	6,996	20,47	6,05E-06	0,0001326	3,87746
HNRPU_HUMAN	150	4,7	145,3	1,274	2,315	20,5	5,96E-06	0,0001326	3,87746
RRP5_HUMAN	27	0	27	Inf	7,014	20,42	6,21E-06	0,0001338	3,87354
LYAR_HUMAN	26,7	0	26,7	Inf	7,002	20,02	7,66E-06	0,0001625	3,78915
PRKDC_HUMAN	50,3	1,3	49	4,112	2,758	19,96	7,90E-06	0,0001629	3,78808
BCLF1_HUMAN	23,3	0	23,3	Inf	6,809	18,82	1,43E-05	0,0002848	3,54546
HP1B3_HUMAN	26,7	0	26,7	Inf	6,98	18,75	1,49E-05	0,0002864	3,54303
TRIPC_HUMAN	22,7	0	22,7	Inf	6,751	18,73	1,51E-05	0,0002864	3,54303

TOP2A_HUMAN	22,3	0	22,3	Inf	6,733	18,74	1,50E-05	0,0002864	3,54303
HSP7C_HUMAN	58,7	2	56,7	3,76	2,429	18,61	1,60E-05	0,0002993	3,52389
POP1_HUMAN	23	0	23	Inf	6,78	18,56	1,65E-05	0,0003043	3,5167
DHX30_HUMAN	28	0	28	Inf	7,073	18,1	2,09E-05	0,0003745	3,42655
RL7_HUMAN	69	2,3	66,7	1,95	2,337	18,12	2,07E-05	0,0003745	3,42655
RL7A_HUMAN	84,3	3,7	80,6	2,026	2,015	17,44	2,97E-05	0,0005103	3,29217
FAS_HUMAN	22,3	0	22,3	Inf	6,723	17,19	3,39E-05	0,0005668	3,24657
ADT2_HUMAN	28,7	0,3	28,4	5,305	3,823	17,19	3,39E-05	0,0005668	3,24657
U2AF5_HUMAN	20,3	0	20,3	Inf	6,606	17,06	3,62E-05	0,0005975	3,22366
PFKAP_HUMAN	20,3	0	20,3	Inf	6,597	16,79	4,18E-05	0,0006818	3,16634
RL26_HUMAN	86	3,7	82,3	2,825	2,131	16,53	4,80E-05	0,0007721	3,11233
RRBP1_HUMAN	22,3	0	22,3	Inf	6,739	16,42	5,08E-05	0,0008077	3,09275
HS90B_HUMAN	131,3	6,7	124,6	2,499	1,884	16,37	5,21E-05	0,0008186	3,08693
RL5_HUMAN	21,7	0	21,7	Inf	6,707	16,26	5,52E-05	0,0008489	3,07114
ADT3_HUMAN	19,3	0	19,3	Inf	6,533	16,25	5,54E-05	0,0008489	3,07114
TBB4A_HUMAN	114,3	7,3	107	1,792	1,49	16,18	5,76E-05	0,0008718	3,05958
RS13_HUMAN	28	0,3	27,7	5,287	3,8	16,15	5,85E-05	0,000875	3,05799
TBB5_HUMAN	173,3	14	159,3	1,51	1,214	16,11	5,99E-05	0,0008852	3,05296
MATR3_HUMAN	21,3	0	21,3	Inf	6,655	15,8	7,05E-05	0,001019	2,99183
SRSF3_HUMAN	19,7	0	19,7	Inf	6,566	15,8	7,03E-05	0,001019	2,99183
FXR1_HUMAN	20	0	20	Inf	6,585	15,64	7,65E-05	0,001081	2,96617
U2AF2_HUMAN	19,3	0	19,3	Inf	6,536	15,62	7,74E-05	0,001081	2,96617
RS3A_HUMAN	90,3	4	86,3	2,4	2,035	15,64	7,67E-05	0,001081	2,96617
NOP58_HUMAN	18,7	0	18,7	Inf	6,48	15,59	7,85E-05	0,001085	2,96457
IF2B3_HUMAN	19	0	19	Inf	6,515	15,56	8,00E-05	0,001094	2,96098
GNL3_HUMAN	22	0	22	Inf	6,693	15,5	8,27E-05	0,001119	2,95117
ATPA_HUMAN	26	0,3	25,7	5,164	3,683	15,32	9,09E-05	0,00121	2,91721
TBB4B_HUMAN	168	14	154	1,818	1,169	15,25	9,43E-05	0,001236	2,90798
TBB2A_HUMAN	141,3	11	130,3	1,378	1,241	15,22	9,55E-05	0,001239	2,90693

NUCL_HUMAN	149,7	9,3	140,4	1,576	1,47	15,07	0,0001036	0,001322	2,87877
COPA_HUMAN	17,7	0	17,7	Inf	6,407	15	0,0001076	0,001356	2,86774
SRPK1_HUMAN	18	0	18	Inf	6,435	14,94	0,000111	0,00137	2,86328
RLA0_HUMAN	43,7	1,3	42,4	3,93	2,581	14,95	0,0001107	0,00137	2,86328
ATPB_HUMAN	25,3	0,3	25	5,125	3,645	14,89	0,000114	0,001394	2,85574
RS24_HUMAN	25,3	0,3	25	5,13	3,649	14,51	0,0001391	0,001685	2,7734
LC7L2_HUMAN	17,7	0	17,7	Inf	6,401	14,43	0,0001458	0,001701	2,7693
RL23_HUMAN	31,7	0,7	31	4,469	3,065	14,24	0,0001611	0,001863	2,72979
LPPRC_HUMAN	16,7	0	16,7	Inf	6,318	14	0,0001828	0,002039	2,69058
FBRL_HUMAN	24,7	0,3	24,4	2,289	3,565	13,88	0,0001944	0,002132	2,67121
RRP12_HUMAN	17,7	0	17,7	Inf	6,386	13,8	0,0002031	0,002208	2,656
AT2A2_HUMAN	16	0	16	Inf	6,26	13,67	0,0002179	0,00231	2,63639
SYEP_HUMAN	16,3	0	16,3	Inf	6,281	13,58	0,0002282	0,002399	2,61997
NOC3L_HUMAN	16	0	16	Inf	6,255	13,31	0,0002636	0,002748	2,56098
RBM28_HUMAN	15,3	0	15,3	Inf	6,202	13,21	0,0002779	0,002861	2,54348
RBM25_HUMAN	15,3	0	15,3	Inf	6,197	13,21	0,0002789	0,002861	2,54348
MBB1A_HUMAN	17	0	17	Inf	6,34	13,09	0,0002976	0,003004	2,5223
CCD86_HUMAN	15,3	0	15,3	Inf	6,194	13,05	0,0003036	0,003041	2,51698
RL31_HUMAN	35,3	1	34,3	2,436	2,605	13,01	0,0003094	0,003074	2,5123
RL12_HUMAN	50,3	2	48,3	1,964	2,129	12,97	0,0003171	0,003127	2,50487
RL27A_HUMAN	22,7	0,3	22,4	4,98	3,495	12,88	0,0003319	0,003223	2,49174
PUF60_HUMAN	15	0	15	Inf	6,167	12,75	0,0003553	0,003398	2,46878
RS4X_HUMAN	65,3	3	62,3	1,76	1,907	12,57	0,0003924	0,003725	2,42887
RT22_HUMAN	15,3	0	15,3	Inf	6,201	12,52	0,0004022	0,003778	2,42274
SRSF5_HUMAN	14,3	0	14,3	Inf	6,102	12,51	0,000404	0,003778	2,42274
NOP16_HUMAN	14,3	0	14,3	Inf	6,107	12,45	0,0004185	0,003886	2,4105
SMCA5_HUMAN	15,3	0	15,3	Inf	6,184	12,4	0,0004288	0,003898	2,40916
RL32_HUMAN	22	0,3	21,7	4,938	3,453	12,4	0,0004284	0,003898	2,40916
RL10_HUMAN	56,7	3	53,7	1,909	1,751	12,4	0,000429	0,003898	2,40916

IF4A1_HUMAN	26,7	0,7	26	4,205	2,804	12,22	0,0004731	0,004238	2,37284
RS11_HUMAN	48,7	2,3	46,4	2,384	1,912	12,23	0,0004702	0,004238	2,37284
HNRPF_HUMAN	14	0	14	Inf	6,072	12,17	0,0004849	0,004313	2,36522
DYHC1_HUMAN	14,7	0	14,7	Inf	6,133	12,13	0,0004949	0,00437	2,35952
RL30_HUMAN	38	1,3	36,7	2,415	2,332	12,12	0,0004982	0,00437	2,35952
EFTU_HUMAN	14,3	0	14,3	Inf	6,109	12,09	0,0005068	0,004375	2,35902
RL3_HUMAN	107,3	6	101,3	1,646	1,61	12,08	0,000509	0,004375	2,35902
TR150_HUMAN	15	0	15	Inf	6,189	11,9	0,0005607	0,004786	2,32003
EF1A1_HUMAN	46,3	2,3	44	3,194	1,869	11,78	0,0005986	0,005043	2,29731
TBA1B_HUMAN	132,3	11	121,3	1,543	1,131	11,73	0,0006157	0,005152	2,28802
SRP68_HUMAN	13,7	0	13,7	Inf	6,034	11,7	0,0006238	0,005187	2,28508
DHX15_HUMAN	14,7	0	14,7	Inf	6,15	11,65	0,0006414	0,005298	2,27589
PGAM5_HUMAN	14,7	0	14,7	Inf	6,146	11,59	0,0006632	0,005407	2,26704
LARP1_HUMAN	14,3	0	14,3	Inf	6,118	11,59	0,0006631	0,005407	2,26704
RBM39_HUMAN	13,3	0	13,3	Inf	6,006	11,54	0,0006804	0,005513	2,25861
XRCC5_HUMAN	20,3	0,3	20	4,804	3,33	11,38	0,0007431	0,005982	2,22315
NUMA1_HUMAN	13,3	0	13,3	Inf	5,998	11,3	0,0007738	0,00619	2,20831
HNRPQ_HUMAN	14,7	0	14,7	Inf	6,162	11,2	0,0008198	0,006518	2,18589
MCM7_HUMAN	13	0	13	Inf	5,96	11,17	0,0008333	0,006584	2,18151
XRCC6_HUMAN	20	0,3	19,7	4,792	3,312	11,15	0,0008392	0,006589	2,18118
RT09_HUMAN	13	0	13	Inf	5,966	11,05	0,0008889	0,006937	2,15883
SRSF2_HUMAN	20,7	0,3	20,4	4,832	3,359	10,89	0,0009654	0,007442	2,12831
STAU1_HUMAN	12,3	0	12,3	Inf	5,894	10,84	0,0009949	0,007623	2,11787
TBA4A_HUMAN	107	8,7	98,3	1,571	1,166	10,61	0,001122	0,008548	2,06814
TBA1A_HUMAN	129	11	118	1,507	1,095	10,52	0,001179	0,008875	2,05183
PR40A_HUMAN	12	0	12	Inf	5,853	10,36	0,001286	0,009512	2,02173
TBB8_HUMAN	62,3	4	58,3	1,853	1,492	10,31	0,001326	0,009751	2,01095
RL38_HUMAN	12	0	12	Inf	5,855	10,26	0,001356	0,009912	2,00384
TBA1C_HUMAN	116,3	9,3	107	1,475	1,162	10,25	0,001365	0,009923	2,00336

CAVN1_HUMAN	11,7	0	11,7	Inf	5,811	10,08	0,001496	0,01063	1,97347
NSUN2_HUMAN	11,7	0	11,7	Inf	5,815	10,01	0,001561	0,01103	1,95742
QCR2_HUMAN	11,7	0	11,7	Inf	5,805	9,985	0,001578	0,01109	1,95507
IF2B2_HUMAN	11,3	0	11,3	Inf	5,775	9,9	0,001653	0,01155	1,93742
RRS1_HUMAN	11,3	0	11,3	Inf	5,779	9,808	0,001737	0,01201	1,92046
UHRF1_HUMAN	11	0	11	Inf	5,732	9,785	0,001759	0,0121	1,91721
DDX18_HUMAN	11	0	11	Inf	5,726	9,768	0,001776	0,01214	1,91578
RL9_HUMAN	12,3	0	12,3	Inf	5,896	9,722	0,001821	0,01239	1,90693
RS25_HUMAN	11,7	0	11,7	Inf	5,819	9,623	0,001922	0,01283	1,89177
ERH_HUMAN	11,3	0	11,3	Inf	5,768	9,609	0,001936	0,01283	1,89177
RL36A_HUMAN	18,7	0,3	18,4	1,906	3,167	9,632	0,001912	0,01283	1,89177
RS18_HUMAN	28,3	1	27,3	3,727	2,36	9,609	0,001936	0,01283	1,89177
DDX3X_HUMAN	49,3	2,7	46,6	1,79	1,713	9,618	0,001926	0,01283	1,89177
BMS1_HUMAN	11,7	0	11,7	Inf	5,814	9,574	0,001974	0,01301	1,88572
PRP8_HUMAN	11	0	11	Inf	5,723	9,38	0,002194	0,01438	1,84224
DDX10_HUMAN	10,7	0	10,7	Inf	5,683	9,365	0,002212	0,01443	1,84073
NOM1_HUMAN	10,3	0	10,3	Inf	5,638	9,222	0,002391	0,01544	1,81135
AT1A1_HUMAN	11,7	0	11,7	Inf	5,788	9,14	0,0025	0,0159	1,7986
NOG1_HUMAN	10	0	10	Inf	5,599	8,896	0,002857	0,0179	1,74715
DNJC9_HUMAN	10,3	0	10,3	Inf	5,63	8,843	0,002942	0,01835	1,73636
EF1G_HUMAN	10	0	10	Inf	5,589	8,823	0,002974	0,01845	1,734
SPS2L_HUMAN	10,3	0	10,3	Inf	5,634	8,783	0,00304	0,01877	1,72654
KRR1_HUMAN	11	0	11	Inf	5,708	8,755	0,003087	0,01897	1,72193
NOG2_HUMAN	9,7	0	9,7	Inf	5,545	8,674	0,003229	0,01974	1,70465
TCPD_HUMAN	9,7	0	9,7	Inf	5,547	8,556	0,003443	0,02096	1,67861
SSF1_HUMAN	9,3	0	9,3	Inf	5,496	8,413	0,003726	0,02257	1,64647
RENT1_HUMAN	9,3	0	9,3	Inf	5,501	8,378	0,003798	0,0229	1,64016
EBP2_HUMAN	11	0	11	Inf	5,76	8,227	0,004126	0,02476	1,60625
PARP1_HUMAN	11	0	11	Inf	5,755	8,182	0,004231	0,02526	1,59757
RL35A_HUMAN	15,7	0,3	15,4	4,439	2,964	8,172	0,004255	0,02529	1,59705

FXR2_HUMAN	9,3	0	9,3	Inf	5,491	8,122	0,004373	0,02563	1,59125
MOV10_HUMAN	9	0	9	Inf	5,446	8,128	0,004359	0,02563	1,59125
ROA0_HUMAN	15,7	0,3	15,4	4,446	2,968	8,136	0,004338	0,02563	1,59125
RL22L_HUMAN	9	0	9	Inf	5,446	7,973	0,004749	0,02758	1,55941
TCPG_HUMAN	9	0	9	Inf	5,437	7,881	0,004995	0,02862	1,54333
DDX54_HUMAN	16	0,3	15,7	1,685	2,946	7,887	0,004978	0,02862	1,54333
QCR1_HUMAN	9	0	9	Inf	5,436	7,869	0,005029	0,02869	1,54227
U520_HUMAN	10	0	10	Inf	5,596	7,822	0,00516	0,0293	1,53313
RS7_HUMAN	34,3	1,7	32,6	3,266	1,952	7,792	0,005248	0,02967	1,52768
DDX47_HUMAN	8,7	0	8,7	Inf	5,397	7,746	0,005384	0,0303	1,51856
RBMX_HUMAN	20	0,7	19,3	3,794	2,4	7,732	0,005424	0,03039	1,51727
TCPA_HUMAN	8,7	0	8,7	Inf	5,397	7,699	0,005526	0,03083	1,51103
RS27_HUMAN	20,3	0,7	19,6	1,808	2,365	7,677	0,005593	0,03107	1,50766
SDA1_HUMAN	8,7	0	8,7	Inf	5,389	7,636	0,00572	0,03164	1,49976
SMN_HUMAN	8,3	0	8,3	Inf	5,333	7,556	0,005981	0,03277	1,48452
HNRPR_HUMAN	15	0,3	14,7	4,393	2,912	7,55	0,006002	0,03277	1,48452
H90B2_HUMAN	23,7	1	22,7	3,435	2,078	7,538	0,00604	0,03283	1,48373
SYRC_HUMAN	8,3	0	8,3	Inf	5,338	7,508	0,006143	0,03325	1,47821
NHP2_HUMAN	8,3	0	8,3	Inf	5,344	7,489	0,006209	0,03332	1,4773
MK67I_HUMAN	8,3	0	8,3	Inf	5,331	7,489	0,006208	0,03332	1,4773
BRX1_HUMAN	8,3	0	8,3	Inf	5,338	7,441	0,006376	0,03408	1,4675
RL26L_HUMAN	49,7	3	46,7	2,219	1,621	7,423	0,006438	0,03424	1,46547
TBB6_HUMAN	38,3	2,3	36	2,04	1,571	7,417	0,006461	0,03424	1,46547
LUC7L_HUMAN	8,3	0	8,3	Inf	5,336	7,407	0,006498	0,0343	1,46471
SPB1_HUMAN	8,3	0	8,3	Inf	5,349	7,357	0,006679	0,03511	1,45457
IF4G1_HUMAN	8,3	0	8,3	Inf	5,324	7,335	0,006764	0,03541	1,45087
TSR1_HUMAN	8,3	0	8,3	Inf	5,353	7,304	0,00688	0,03587	1,44527
DDX52_HUMAN	8	0	8	Inf	5,287	7,159	0,007457	0,03773	1,42331
DDX56_HUMAN	8	0	8	Inf	5,274	7,167	0,007424	0,03773	1,42331

AP3D1_HUMAN	9,3	0	9,3	Inf	5,489	7,136	0,007556	0,03799	1,42033
PCBP2_HUMAN	8	0	8	Inf	5,281	7,121	0,007619	0,03816	1,41839
TF3C1_HUMAN	8	0	8	Inf	5,279	7,075	0,007816	0,03884	1,41072
CC137_HUMAN	8	0	8	Inf	5,271	7,068	0,007847	0,03884	1,41072
SYMC_HUMAN	8	0	8	Inf	5,293	6,957	0,008351	0,04058	1,39169
RL22_HUMAN	8	0	8	Inf	5,282	6,955	0,008359	0,04058	1,39169
DKC1_HUMAN	7,7	0	7,7	Inf	5,223	6,957	0,008348	0,04058	1,39169
RS20_HUMAN	14,3	0,3	14	4,29	2,831	6,885	0,008691	0,04203	1,37644
RSSA_HUMAN	7,7	0	7,7	Inf	5,218	6,814	0,009043	0,0434	1,36251
TF3C3_HUMAN	7,7	0	7,7	Inf	5,213	6,777	0,009235	0,044	1,35655
SNUT1_HUMAN	7,7	0	7,7	Inf	5,209	6,78	0,009217	0,044	1,35655
RS23_HUMAN	34,7	2	32,7	1,424	1,591	6,702	0,009631	0,04571	1,33999
SLTM_HUMAN	7,3	0	7,3	Inf	5,167	6,538	0,01056	0,04961	1,30443
TBA4B_HUMAN	7,3	0	7,3	Inf	5,162	6,536	0,01057	0,04961	1,30443

Table 2: List of significantly enriched proteins in SINV-DDX5_IP versus SINV-IgG_IP

1st column : Protein name
2nd column : Column named as the treatment level with the mean raw spectral counts observed for this condition
3rd column : Column named as the control level with the mean raw spectral counts observed for this condition

deltaSC : Difference between mean raw spectral counts
lFC.Av : Log fold change computed from the mean expression levels taking into account the given normalization factors.
logFC : Log fold change estimated by fitting the given GLM model. The reference level of the main factor is taken as control.

LR : The likelihood ratio for edgeR.

p.val : The unadjusted p-values obtained from the tests.

adjp : The multitest adjusted p-values with FDR control.

	SINV_DDX5IP	SINV_IgGIP	deltaSC	lFC_Av	LogFC	LR	p_value	adjp	negLog_adjp
DDX5_HUMAN	717,3	0,3	717	9,588	8,422	157,9	3,17E-36	3,87E-33	32,41274
DDX21_HUMAN	137,3	0,7	136,6	6,197	5,12	55,9	7,61E-14	4,64E-11	10,33386
DDX17_HUMAN	115,3	0,3	115	6,94	5,776	54,24	1,77E-13	7,20E-11	10,14285
RL6_HUMAN	89,7	0,3	89,4	6,578	5,414	44,59	2,42E-11	7,38E-09	8,13183
YBOX1_HUMAN	138	2	136	3,513	3,568	40,57	1,90E-10	4,62E-08	7,33564
SRRM2_HUMAN	66,3	0	66,3	Inf	8,314	37,75	8,05E-10	1,64E-07	6,78648
YBOX3_HUMAN	51	0	51	Inf	7,924	32,25	1,36E-08	1,84E-06	5,73565
RL36_HUMAN	48,7	0	48,7	Inf	7,849	31,72	1,78E-08	2,08E-06	5,68298
SRRM1_HUMAN	42,7	0	42,7	Inf	7,665	28,78	8,11E-08	7,60E-06	5,11942
KI67_HUMAN	47,3	0	47,3	Inf	7,816	28,19	1,10E-07	8,83E-06	5,05384
RL35_HUMAN	43	0	43	Inf	7,684	28,2	1,09E-07	8,83E-06	5,05384
RS6_HUMAN	84	1,7	82,3	4,158	3,167	28,09	1,16E-07	8,83E-06	5,05384
RL21_HUMAN	42,7	0	42,7	Inf	7,669	27,36	1,69E-07	1,14E-05	4,94271
NOP56_HUMAN	54	0,3	53,7	5,883	4,728	24,71	6,66E-07	3,90E-05	4,40905
RL18A_HUMAN	62,7	1	61,7	4,458	3,428	24,69	6,72E-07	3,90E-05	4,40905
PNPT1_HUMAN	48	0	48	Inf	7,879	23,35	1,35E-06	6,84E-05	4,16494
RS13_HUMAN	29,7	0	29,7	Inf	7,131	21,28	3,96E-06	0,0001776	3,75056
RL13A_HUMAN	47,7	0,7	47	4,675	3,604	21,23	4,07E-06	0,0001776	3,75056

RL17_HUMAN	56,7	1	55,7	4,349	3,321	21,31	3,91E-06	0,0001776	3,75056
PABP1_HUMAN	70,7	1,7	69	3,932	2,958	21,16	4,23E-06	0,0001776	3,75056
Pol_S_SINV_Capside	119	5	114	2,229	2,061	21,19	4,16E-06	0,0001776	3,75056
NUCL_HUMAN	163,3	5,3	158	3,446	2,715	20,72	5,31E-06	0,0002086	3,68069
LYAR_HUMAN	28,3	0	28,3	Inf	7,069	20,37	6,38E-06	0,0002429	3,61457
RS4X_HUMAN	72,3	2	70,3	3,696	2,739	19,93	8,02E-06	0,0002958	3,529
NAT10_HUMAN	36,3	0,3	36	5,275	4,117	19,51	9,99E-06	0,0003405	3,46788
NOP2_HUMAN	53,3	1	52,3	4,262	3,238	19,5	1,01E-05	0,0003405	3,46788
POP1_HUMAN	26,3	0	26,3	Inf	6,975	19,05	1,28E-05	0,00042	3,37675
RL5_HUMAN	26,7	0	26,7	Inf	6,983	18,62	1,60E-05	0,0004856	3,31372
BCLF1_HUMAN	25	0	25	Inf	6,886	18,67	1,55E-05	0,0004856	3,31372
TOP1_HUMAN	35	0,3	34,7	5,226	4,068	18,64	1,58E-05	0,0004856	3,31372
RRP1B_HUMAN	26,3	0	26,3	Inf	6,961	18,56	1,65E-05	0,0004885	3,31114
SRP72_HUMAN	23,7	0	23,7	Inf	6,818	17,76	2,51E-05	0,0006977	3,15633
HSP7C_HUMAN	67,3	2	65,3	3,108	2,597	17,75	2,52E-05	0,0006977	3,15633
HNRPU_HUMAN	166	9	157	1,96	1,782	17,83	2,41E-05	0,0006977	3,15633
RRP12_HUMAN	22,7	0	22,7	Inf	6,75	17,31	3,18E-05	0,0008066	3,09334
RL10_HUMAN	63,7	2	61,7	3,478	2,518	17,32	3,16E-05	0,0008066	3,09334
MBB1A_HUMAN	23,7	0	23,7	Inf	6,841	16,86	4,03E-05	0,0009999	3,00004
RL10A_HUMAN	63,7	2	61,7	3,506	2,553	16,82	4,11E-05	0,0009999	3,00004
DHX30_HUMAN	23,3	0	23,3	Inf	6,793	16,66	4,46E-05	0,001066	2,97224
RS7_HUMAN	31,3	0,3	31	5,071	3,914	16,55	4,73E-05	0,001108	2,95546
GNL3_HUMAN	21,7	0	21,7	Inf	6,696	16,37	5,22E-05	0,001178	2,92885
NOP58_HUMAN	21,3	0	21,3	Inf	6,661	16,4	5,14E-05	0,001178	2,92885
ATPB_HUMAN	21,3	0	21,3	Inf	6,66	16,18	5,76E-05	0,001274	2,89483
RRP5_HUMAN	21	0	21	Inf	6,634	16,14	5,89E-05	0,001281	2,89245
RL7A_HUMAN	90,3	3,7	86,6	3,135	2,28	16,09	6,05E-05	0,001293	2,8884
NUMA1_HUMAN	22,7	0	22,7	Inf	6,727	15,92	6,62E-05	0,001319	2,87976
RL27_HUMAN	29,3	0,3	29	4,965	3,81	15,52	8,16E-05	0,001553	2,80883

RBM28_HUMAN	21,3	0	21,3	Inf	6,69	15,29	9,24E-05	0,001679	2,77495
U2AF5_HUMAN	19,3	0	19,3	Inf	6,524	15,08	0,0001033	0,00185	2,73283
TOP2A_HUMAN	20	0	20	Inf	6,594	15,03	0,000106	0,001871	2,72793
PABP4_HUMAN	36	0,7	35,3	4,281	3,215	14,97	0,0001091	0,001871	2,72793
DDX24_HUMAN	31	0,3	30,7	5,025	3,882	14,84	0,000117	0,00198	2,70333
RL27A_HUMAN	28,7	0,3	28,4	4,906	3,761	14,78	0,0001206	0,002012	2,69637
RL7_HUMAN	70,3	2,3	68	3,46	2,571	14,65	0,0001294	0,002129	2,67182
MATR3_HUMAN	18,7	0	18,7	Inf	6,477	14,4	0,000148	0,002404	2,61907
HP1B3_HUMAN	22	0	22	Inf	6,744	14,3	0,0001561	0,002447	2,61137
DHX15_HUMAN	19,7	0	19,7	Inf	6,559	14,31	0,000155	0,002447	2,61137
RLA2_HUMAN	40,3	1	39,3	2,513	2,76	14,29	0,0001567	0,002447	2,61137
IF2B3_HUMAN	18,3	0	18,3	Inf	6,458	14,18	0,0001662	0,002499	2,60223
RRBP1_HUMAN	18	0	18	Inf	6,431	14,01	0,0001819	0,002702	2,56831
RL18_HUMAN	68	2,7	65,3	3,203	2,306	13,98	0,0001846	0,002709	2,56719
FXR1_HUMAN	17,7	0	17,7	Inf	6,405	13,85	0,0001982	0,002874	2,54151
SRSF3_HUMAN	17,7	0	17,7	Inf	6,389	13,75	0,0002087	0,002967	2,52768
RS11_HUMAN	48,7	1,7	47	3,385	2,407	13,69	0,0002156	0,003018	2,52028
EBP2_HUMAN	17,3	0	17,3	Inf	6,387	13,42	0,0002493	0,0033	2,48149
AT2A2_HUMAN	17	0	17	Inf	6,342	13,42	0,000249	0,0033	2,48149
RL4_HUMAN	188,3	7,3	181	3,203	2,664	13,42	0,0002483	0,0033	2,48149
RRS1_HUMAN	17,7	0	17,7	Inf	6,401	13,37	0,0002561	0,003335	2,4769
COPA_HUMAN	17	0	17	Inf	6,351	13,36	0,0002574	0,003335	2,4769
RL26_HUMAN	97	5	92	2,583	1,953	13,12	0,0002916	0,003738	2,42736
SMCA5_HUMAN	17,7	0	17,7	Inf	6,418	13,09	0,0002962	0,003758	2,42504
RL3_HUMAN	111,3	6,7	104,6	1,909	1,63	13,02	0,0003086	0,003835	2,41623
SRP68_HUMAN	16,7	0	16,7	Inf	6,333	12,83	0,000341	0,004195	2,37727
PRKDC_HUMAN	50,3	2	48,3	3,164	2,204	12,62	0,0003822	0,004609	2,33639
NOP16_HUMAN	16	0	16	Inf	6,264	12,53	0,0004013	0,004793	2,31939
DDX3X_HUMAN	42	1,3	40,7	3,504	2,516	12,32	0,0004475	0,005278	2,27753

XRCC5_HUMAN	16,7	0	16,7	Inf	6,275	12,22	0,0004729	0,005433	2,26496
BMS1_HUMAN	15,7	0	15,7	Inf	6,243	12,23	0,0004712	0,005433	2,26496
RLA0_HUMAN	44	1,7	42,3	3,227	2,246	12,1	0,0005041	0,005739	2,24116
HNRPQ_HUMAN	15,7	0	15,7	Inf	6,214	12,05	0,0005183	0,005845	2,23322
RS3A_HUMAN	94,7	5,3	89,4	2,457	1,819	12,02	0,000525	0,005867	2,23158
DKC1_HUMAN	15,3	0	15,3	Inf	6,198	11,98	0,0005368	0,005944	2,22592
SRPK1_HUMAN	15,7	0	15,7	Inf	6,235	11,94	0,0005507	0,006043	2,21875
CCD86_HUMAN	15,3	0	15,3	Inf	6,209	11,85	0,0005762	0,006266	2,20301
RL36A_HUMAN	23	0,3	22,7	4,619	3,467	11,77	0,000602	0,006488	2,18789
Pol_NS_SINV_nsP2	28,7	0,7	28	3,922	2,86	11,75	0,0006083	0,006499	2,18715
SPS2L_HUMAN	14,7	0	14,7	Inf	6,141	11,69	0,0006292	0,006664	2,17627
RL12_HUMAN	40	1,3	38,7	3,439	2,448	11,67	0,000635	0,006667	2,17607
IMA1_HUMAN	22,7	0,3	22,4	4,597	3,445	11,64	0,0006443	0,006707	2,17347
PFKAP_HUMAN	22,7	0,3	22,4	4,603	3,449	11,61	0,0006544	0,006755	2,17037
TR150_HUMAN	15,3	0	15,3	Inf	6,192	11,56	0,0006725	0,006883	2,16222
RL14_HUMAN	37,7	1	36,7	1,746	2,604	11,54	0,0006822	0,006924	2,15964
RL1D1_HUMAN	46	1,7	44,3	3,292	2,337	11,51	0,0006941	0,006987	2,15571
U2AF2_HUMAN	15	0	15	Inf	6,189	11,47	0,000709	0,00702	2,15366
NOG1_HUMAN	14,7	0	14,7	Inf	6,16	11,37	0,0007483	0,007291	2,13721
MCM7_HUMAN	14,7	0	14,7	Inf	6,109	11,34	0,0007598	0,007345	2,13401
HNRPR_HUMAN	14,7	0	14,7	Inf	6,112	11,25	0,0007953	0,007509	2,12442
RBMX_HUMAN	22	0,3	21,7	4,544	3,395	11,26	0,0007916	0,007509	2,12442
RL26L_HUMAN	58,7	3	55,7	2,46	1,847	10,92	0,0009535	0,008602	2,0654
DDX54_HUMAN	13,3	0	13,3	Inf	6	10,83	0,0009971	0,008868	2,05217
RS16_HUMAN	37,3	1,3	36	3,292	2,3	10,83	0,0009975	0,008868	2,05217
PUF60_HUMAN	13,3	0	13,3	Inf	6,003	10,8	0,001014	0,00895	2,04818
HS90A_HUMAN	71,7	3,7	68	2,778	1,945	10,67	0,001087	0,009527	2,02104
SRSF5_HUMAN	13,3	0	13,3	Inf	6,02	10,56	0,001158	0,01	2
DDX18_HUMAN	13	0	13	Inf	5,96	10,48	0,00121	0,01031	1,98674

EFTU_HUMAN	13	0	13	Inf	5,947	10,47	0,00121	0,01031	1,98674
RT22_HUMAN	13,3	0	13,3	Inf	6,019	10,45	0,001226	0,01037	1,98422
KRR1_HUMAN	13,3	0	13,3	Inf	5,993	10,32	0,001313	0,01086	1,96417
RL30_HUMAN	37,7	1,3	36,4	3,36	2,38	10,32	0,001319	0,01086	1,96417
ATD3A_HUMAN	13,7	0	13,7	Inf	5,992	10,15	0,001446	0,01159	1,93592
BRX1_HUMAN	12,7	0	12,7	Inf	5,908	10,07	0,001508	0,01185	1,92628
AT1A1_HUMAN	12,3	0	12,3	Inf	5,889	10,07	0,001503	0,01185	1,92628
RT09_HUMAN	12,3	0	12,3	Inf	5,891	10,04	0,001534	0,0119	1,92445
DNJC9_HUMAN	12,3	0	12,3	Inf	5,889	10,05	0,001525	0,0119	1,92445
CAVN1_HUMAN	12,3	0	12,3	Inf	5,882	10,01	0,001554	0,01198	1,92154
PGAM5_HUMAN	12,3	0	12,3	Inf	5,881	9,983	0,00158	0,0121	1,91721
RL35A_HUMAN	12,3	0	12,3	Inf	5,902	9,905	0,001649	0,01247	1,90413
RACK1_HUMAN	25,7	0,7	25	3,755	2,7	9,916	0,001638	0,01247	1,90413
SRSF2_HUMAN	19,7	0,3	19,4	4,372	3,23	9,755	0,001788	0,01344	1,8716
DYHC1_HUMAN	11,7	0	11,7	Inf	5,807	9,634	0,00191	0,01427	1,84558
DHX9_HUMAN	30,3	1	29,3	3,455	2,438	9,558	0,001991	0,01479	1,83003
RL8_HUMAN	58	3,3	54,7	1,867	1,633	9,484	0,002072	0,0153	1,81531
LC7L2_HUMAN	19,7	0,3	19,4	4,405	3,256	9,449	0,002113	0,0155	1,80967
IF2B2_HUMAN	11,7	0	11,7	Inf	5,797	9,38	0,002194	0,016	1,79588
TRIPC_HUMAN	19	0,3	18,7	4,341	3,192	9,368	0,002208	0,01601	1,79561
STAU1_HUMAN	11,3	0	11,3	Inf	5,773	9,182	0,002445	0,01762	1,75399
NOM1_HUMAN	11	0	11	Inf	5,726	9,124	0,002522	0,01807	1,74304
RL38_HUMAN	11,3	0	11,3	Inf	5,752	9,112	0,002539	0,01809	1,74256
SPB1_HUMAN	11,7	0	11,7	Inf	5,832	9,09	0,00257	0,01812	1,74184
RL23_HUMAN	29,7	1	28,7	3,362	2,355	9,087	0,002574	0,01812	1,74184
U520_HUMAN	11	0	11	Inf	5,742	8,984	0,002724	0,01907	1,71965
RL36L_HUMAN	18,3	0,3	18	4,312	3,159	8,867	0,002904	0,02021	1,69443
LARP1_HUMAN	11	0	11	Inf	5,708	8,818	0,002982	0,02064	1,68529
SSF1_HUMAN	10,7	0	10,7	Inf	5,693	8,806	0,003003	0,02067	1,68466

DDX10_HUMAN	10,7	0	10,7	Inf	5,698	8,705	0,003174	0,02172	1,66314
SYRC_HUMAN	10,3	0	10,3	Inf	5,651	8,522	0,003509	0,02374	1,62452
RRP1_HUMAN	10	0	10	Inf	5,596	8,366	0,003824	0,02573	1,58956
TSR1_HUMAN	10	0	10	Inf	5,58	8,269	0,004034	0,02699	1,5688
MK67I_HUMAN	10	0	10	Inf	5,594	8,252	0,004071	0,0271	1,56703
HNRL1_HUMAN	18	0,3	17,7	4,305	3,155	8,238	0,004102	0,02715	1,56623
SDA1_HUMAN	10	0	10	Inf	5,595	8,123	0,004371	0,02854	1,54455
NHP2_HUMAN	9,7	0	9,7	Inf	5,545	8,119	0,004381	0,02854	1,54455
RS9_HUMAN	31,3	1,3	30	3,032	2,049	8,087	0,004458	0,02888	1,5394
RT18B_HUMAN	9,7	0	9,7	Inf	5,538	8,045	0,004562	0,02935	1,53239
RS18_HUMAN	30,3	1,3	29	3,022	2,025	8,039	0,004578	0,02935	1,53239
XRCC6_HUMAN	21,7	0,7	21	3,508	2,456	7,896	0,004954	0,03159	1,50045
FIP1_HUMAN	9,7	0	9,7	Inf	5,551	7,833	0,00513	0,03187	1,49662
IF4G1_HUMAN	9,3	0	9,3	Inf	5,501	7,806	0,005208	0,03187	1,49662
UHRF1_HUMAN	9,3	0	9,3	Inf	5,499	7,808	0,005203	0,03187	1,49662
TCPG_HUMAN	9,3	0	9,3	Inf	5,486	7,853	0,005074	0,03187	1,49662
ADT2_HUMAN	30,7	1,3	29,4	3,004	2,021	7,818	0,005172	0,03187	1,49662
TCPD_HUMAN	10	0	10	Inf	5,565	7,679	0,005586	0,03368	1,47263
SYEP_HUMAN	16,3	0,3	16	4,091	2,959	7,602	0,005832	0,03459	1,46105
RS2_HUMAN	60,7	4	56,7	2,44	1,616	7,592	0,005864	0,03459	1,46105
NOL10_HUMAN	9	0	9	Inf	5,453	7,523	0,006091	0,0355	1,44977
FBRL_HUMAN	25	1	24	3,153	2,13	7,498	0,006178	0,03583	1,44575
NSUN2_HUMAN	9	0	9	Inf	5,439	7,456	0,006323	0,0365	1,43771
TBB4A_HUMAN	130,7	11,3	119,4	1,217	1,087	7,417	0,00646	0,03712	1,43039
RPF2_HUMAN	9	0	9	Inf	5,427	7,357	0,006679	0,0376	1,42481
RS23_HUMAN	33	1,7	31,3	2,838	1,875	7,223	0,007199	0,04022	1,39556
PR40A_HUMAN	8,7	0	8,7	Inf	5,367	7,196	0,007306	0,04063	1,39115
RS27_HUMAN	20,3	0,7	19,6	3,446	2,389	7,17	0,007415	0,04105	1,38669
RL22L_HUMAN	8,7	0	8,7	Inf	5,371	7,135	0,00756	0,04115	1,38563

PRP6_HUMAN	8,7	0	8,7	Inf	5,367	7,136	0,007557	0,04115	1,38563
KRI1_HUMAN	8,7	0	8,7	Inf	5,39	7,093	0,007737	0,04188	1,37799
RS24_HUMAN	20	0,7	19,3	3,428	2,368	7,049	0,007932	0,04275	1,36906
CC137_HUMAN	8,3	0	8,3	Inf	5,35	7,015	0,008082	0,04327	1,36381
PESC_HUMAN	8,3	0	8,3	Inf	5,33	7,011	0,008101	0,04327	1,36381
TDIF2_HUMAN	8,3	0	8,3	Inf	5,337	6,953	0,008367	0,0445	1,35164
ILF3_HUMAN	24,7	1	23,7	3,167	2,156	6,882	0,008709	0,04592	1,338
LUC7L_HUMAN	8	0	8	Inf	5,281	6,813	0,00905	0,04732	1,32496
F120A_HUMAN	8	0	8	Inf	5,279	6,813	0,009052	0,04732	1,32496
RM11_HUMAN	8	0	8	Inf	5,283	6,784	0,009198	0,04767	1,32175
DDX56_HUMAN	8	0	8	Inf	5,27	6,784	0,009198	0,04767	1,32175
DDX52_HUMAN	8	0	8	Inf	5,287	6,758	0,009335	0,04818	1,31713
RL32_HUMAN	19,3	0,7	18,6	3,359	2,303	6,743	0,009412	0,04837	1,31542
BAG2_HUMAN	8	0	8	Inf	5,298	6,672	0,009794	0,04991	1,30181

Table 3: List of significantly enriched proteins in SINV-DDX5_IP versus mock-DDX5_IP

1st column : Protein name
2nd column : Column named as the treatment level with the mean raw spectral counts observed for this condition
3rd column : Column named as the control level with the mean raw spectral counts observed for this condition

deltaSC : Difference between mean raw spectral counts
lFC.Av : Log fold change computed from the mean expression levels taking into account the given normalization factors.
logFC : Log fold change estimated by fitting the given GLM model. The reference level of the main factor is taken as control.

LR : The likelihood ratio for edgeR.

p.val : The unadjusted p-values obtained from the tests.

adjp : The multitest adjusted p-values with FDR control.

	SINV_DDX5IP	mock_DDX5IP	deltaSC	lFC_Av	LogFC	LR	p_value	adjp	negLog_adjp
Pol_S_SINV_Capside	119	0	119	Inf	9,879	207,9	3,90E-47	5,36E-44	43,27059
Pol_NS_SINV_nsP2	28,7	0	28,7	Inf	7,83	79,84	4,06E-19	2,80E-16	15,55346
Pol_S_SINV_E1	15,3	0	15,3	Inf	6,925	47,44	5,66E-12	2,60E-09	8,58503
Pol_S_SINV_E2	15	0	15	Inf	6,895	46,7	8,27E-12	2,85E-09	8,54561
Pol_NS_SINV_nsP3	14,3	0	14,3	Inf	6,862	43,42	4,42E-11	1,22E-08	7,91435
MYH9_HUMAN	349,7	0,7	349	8,624	8,477	30,21	3,87E-08	8,88E-06	5,05154
MYH10_HUMAN	84,3	0	84,3	Inf	9,136	20,98	4,64E-06	0,000913	3,03953
MYL6_HUMAN	23,7	0,3	23,4	6,06	5,499	18,26	1,93E-05	0,003323	2,47847
MYL6B_HUMAN	5	0	5	Inf	5,292	16,9	3,93E-05	0,006015	2,22076
TPM3_HUMAN	21	0	21	Inf	7,147	14,9	0,0001132	0,01418	1,84832
TPM4_HUMAN	18,7	0	18,7	Inf	6,982	14,72	0,0001246	0,0143	1,84466
MYH11_HUMAN	20,3	0,7	19,6	4,539	4,433	14,28	0,0001573	0,01547	1,81051
TPM2_HUMAN	15,3	0	15,3	Inf	6,706	14,41	0,0001473	0,01547	1,81051
MYH14_HUMAN	21	0	21	Inf	7,139	13,3	0,0002648	0,02279	1,64226
ML12B_HUMAN	7,3	0	7,3	Inf	5,696	12,93	0,000323	0,02616	1,58236
MY18A_HUMAN	12,3	0	12,3	Inf	6,39	12,4	0,0004287	0,0328	1,48413

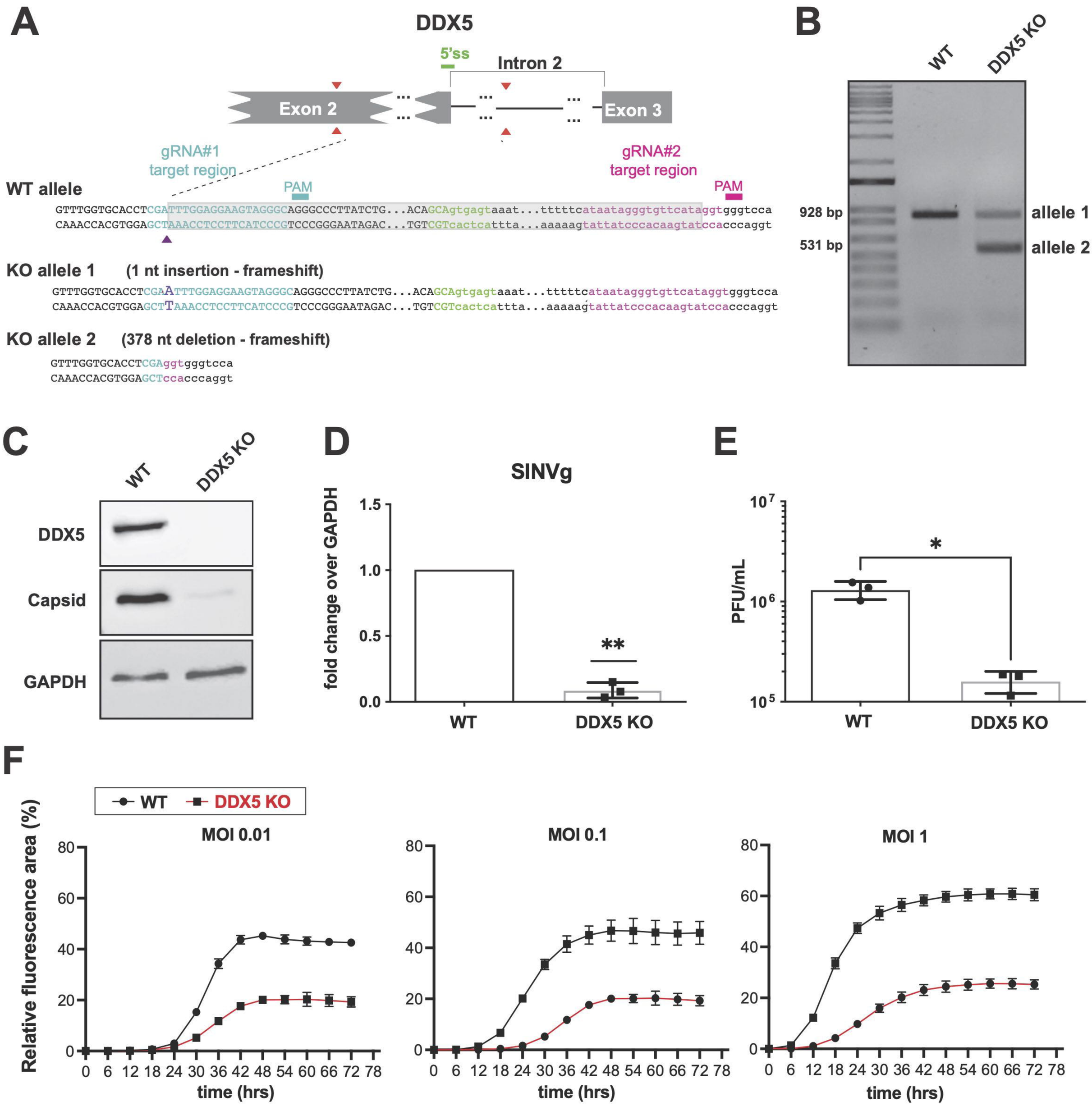
A
DDX5
5'ss
Intron 2
Exon 2
Exon 3
gRNA#1
target region
gRNA#2
target region
PAM
PAM
WT allele
GTTTGGTGCACCTCGATTTGGAGGAAGTAGGGCAGGGCCCTTATCTG...ACAGCAgtgagtaaat...tttttcataatagggtgttcataggtgggtcca
CAAACCACGTGGAGCTAAACCTCCTTCATCCCGTCCCGGGAATAGAC...TGTCGTcactcattta...aaaaagtattatcccacaagtatccacccaggt
KO allele 1 (1 nt insertion - frameshift)
GTTTGGTGCACCTCGAATTTGGAGGAAGTAGGGCAGGGCCCTTATCTG...ACAGCAgtgagtaaat...tttttcataatagggtgttcataggtgggtcca
CAAACCACGTGGAGCTTAAACCTCCTTCATCCCGTCCCGGGAATAGAC...TGTCGTcactcattta...aaaaagtattatcccacaagtatccacccaggt
KO allele 2 (378 nt deletion - frameshift)
GTTTGGTGCACCTCGAggtgggtcca
CAAACCACGTGGAGCTccacccaggt
B
WT
DDX5 KO
928 bp
531 bp
allele 1
allele 2
C
WT
DDX5 KO
DDX5
Capsid
GAPDH
D
SINVg
fold change over GAPDH
1.5
1.0
0.5
0.0
**
WT
DDX5 KO
E
PFU/mL
10^7
10^6
10^5
*
WT
DDX5 KO
F
WT
DDX5 KO
Relative fluorescence area (%)
MOI 0.01
MOI 0.1
MOI 1
80
60
40
20
0
0 6 12 18 24 30 36 42 48 54 60 66 72 78
time (hrs)

Figure 1

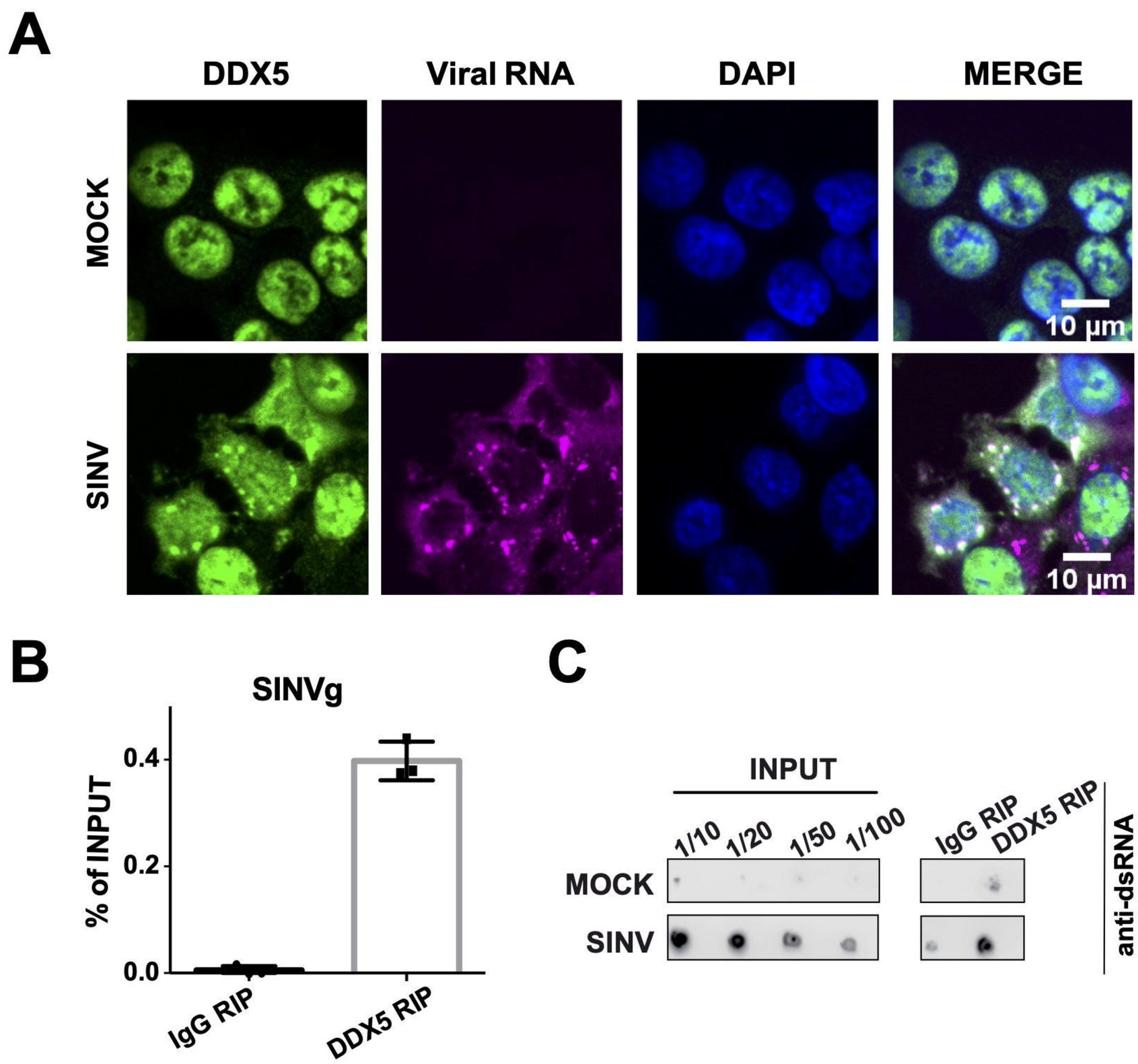
A
DDX5
Viral RNA
DAPI
MERGE
MOCK
SINV
10 µm
10 µm
B
SINVg
% of INPUT
0.4
0.2
0.0
IgG RIP
DDX5 RIP
C
INPUT
1/10
1/20
1/50
1/100
IgG RIP
DDX5 RIP
MOCK
SINV
anti-dsRNA

Figure 2

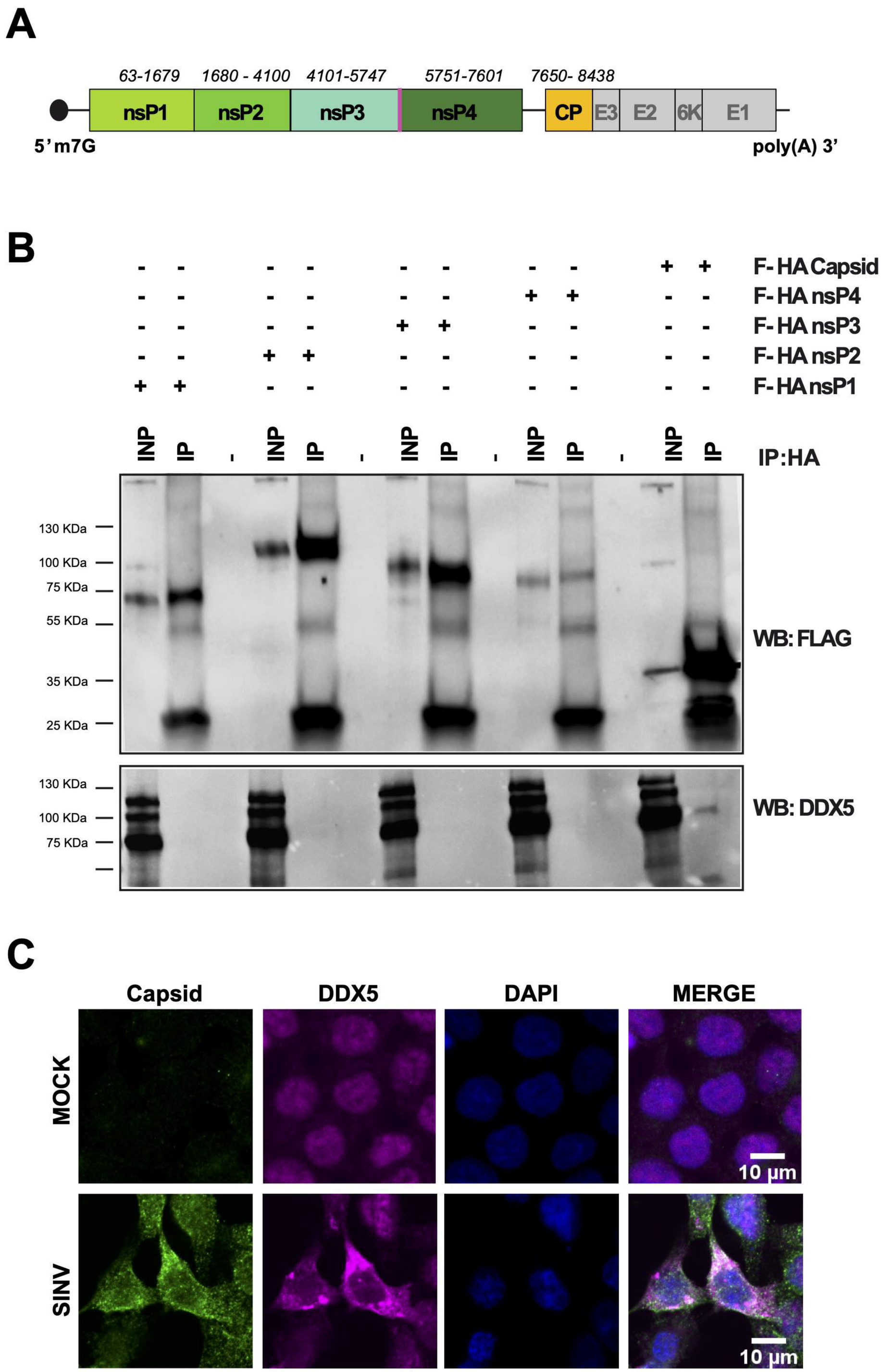
A
63-1679
1680 - 4100
4101-5747
5751-7601
7650- 8438
nsP1
nsP2
nsP3
nsP4
CP
E3
E2
6K
E1
5' m7G
poly(A) 3'
B
F- HA Capsid
F- HA nsP4
F- HA nsP3
F- HA nsP2
F- HA nsP1
INP
IP
IP:HA
130 KDa
100 KDa
75 KDa
55 KDa
35 KDa
25 KDa
WB: FLAG
WB: DDX5
C
Capsid
DDX5
DAPI
MERGE
MOCK
SINV
10 µm

Figure 3

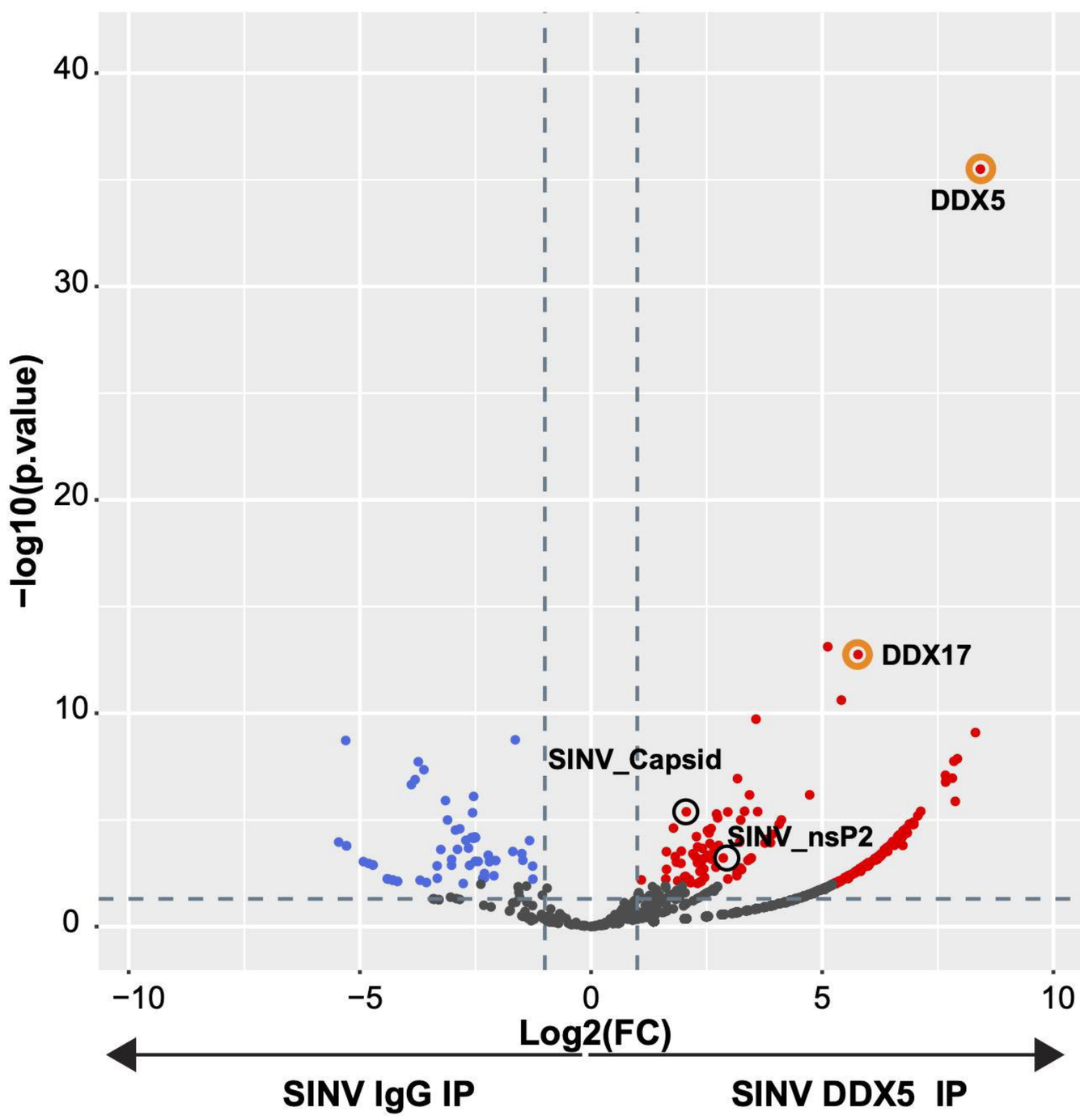
A
40
30
20
10
0
−log10(p.value)
DDX5
DDX17
SINV_Capsid
SINV_nsP2
−10
−5
0
5
10
Log2(FC)
SINV IgG IP
SINV DDX5 IP

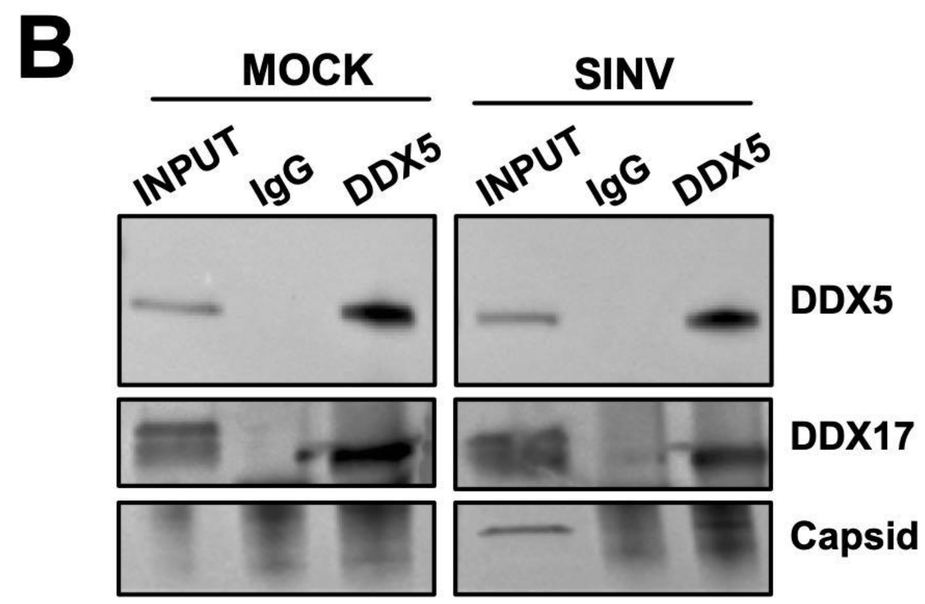
B
MOCK
SINV
INPUT
IgG
DDX5
INPUT
IgG
DDX5
DDX5
DDX17
Capsid

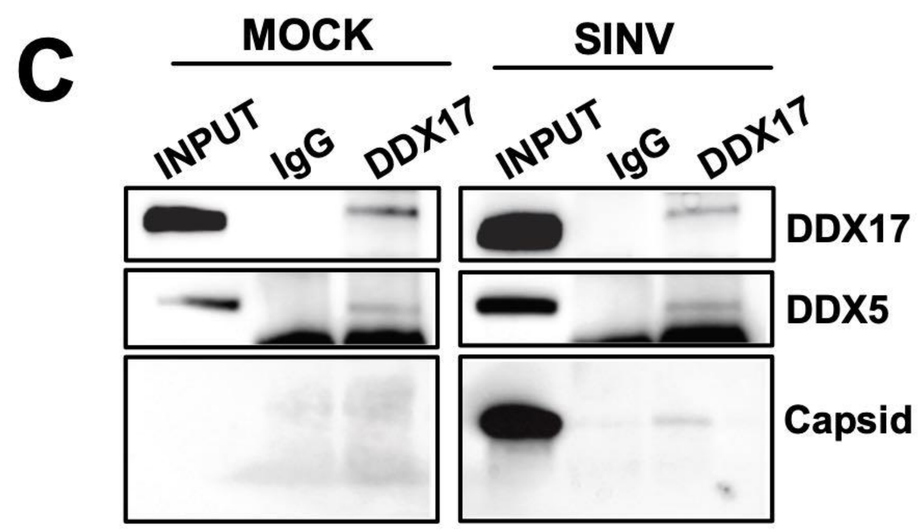
C
MOCK
SINV
INPUT
IgG
DDX17
INPUT
IgG
DDX17
DDX17
DDX5
Capsid

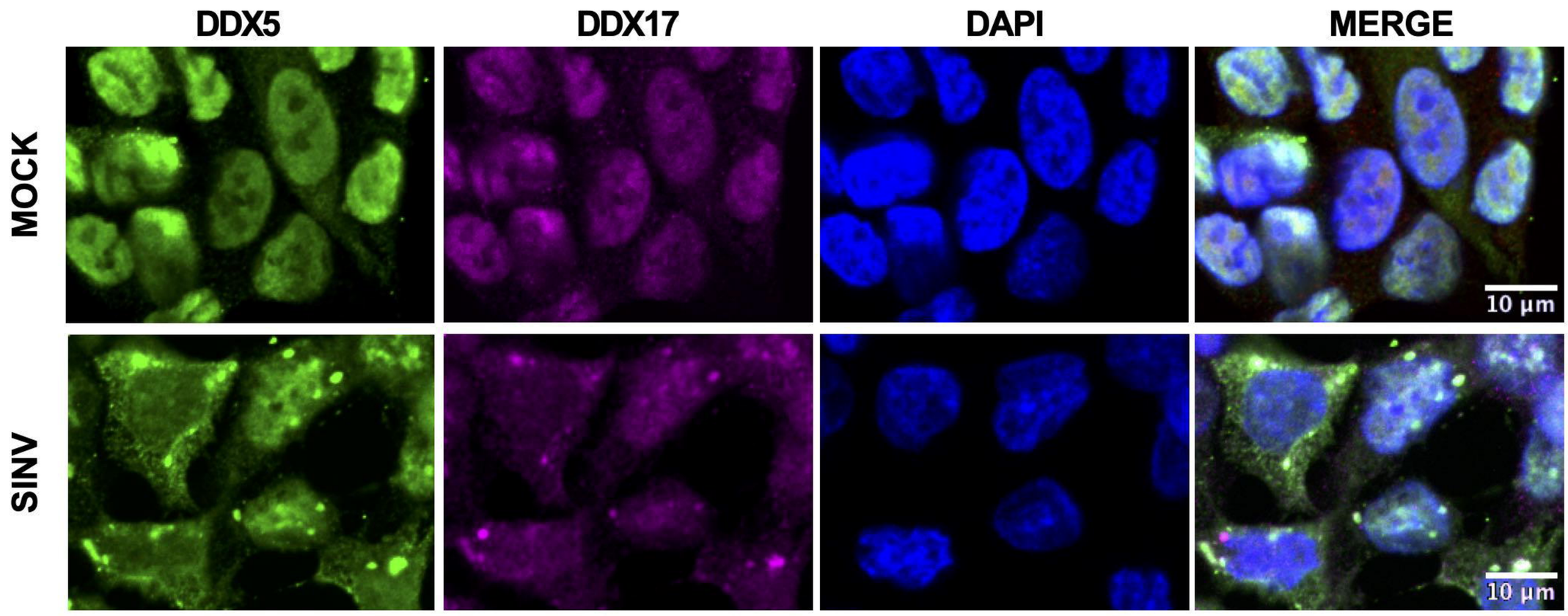
D
DDX5
DDX17
DAPI
MERGE
MOCK
SINV
10 µm
10 µm

Figure 4

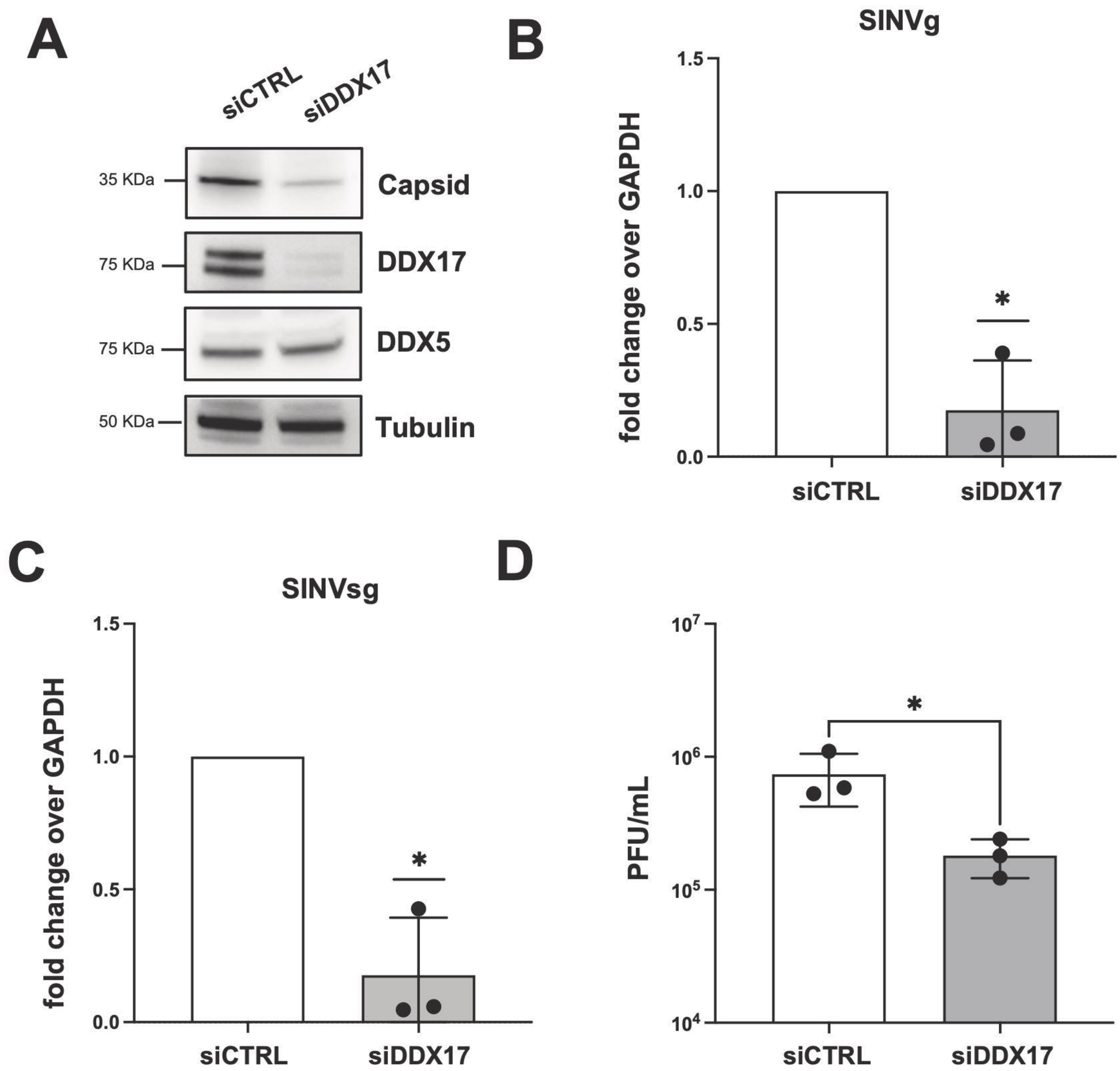
A
siCTRL
siDDX17
35 KDa
Capsid
75 KDa
DDX17
75 KDa
DDX5
50 KDa
Tubulin
B
SINVg
fold change over GAPDH
1.5
1.0
0.5
0.0
*
siCTRL
siDDX17
C
SINVsg
fold change over GAPDH
1.5
1.0
0.5
0.0
*
siCTRL
siDDX17
D
PFU/mL
10^7
10^6
10^5
10^4
*
siCTRL
siDDX17

Figure 5

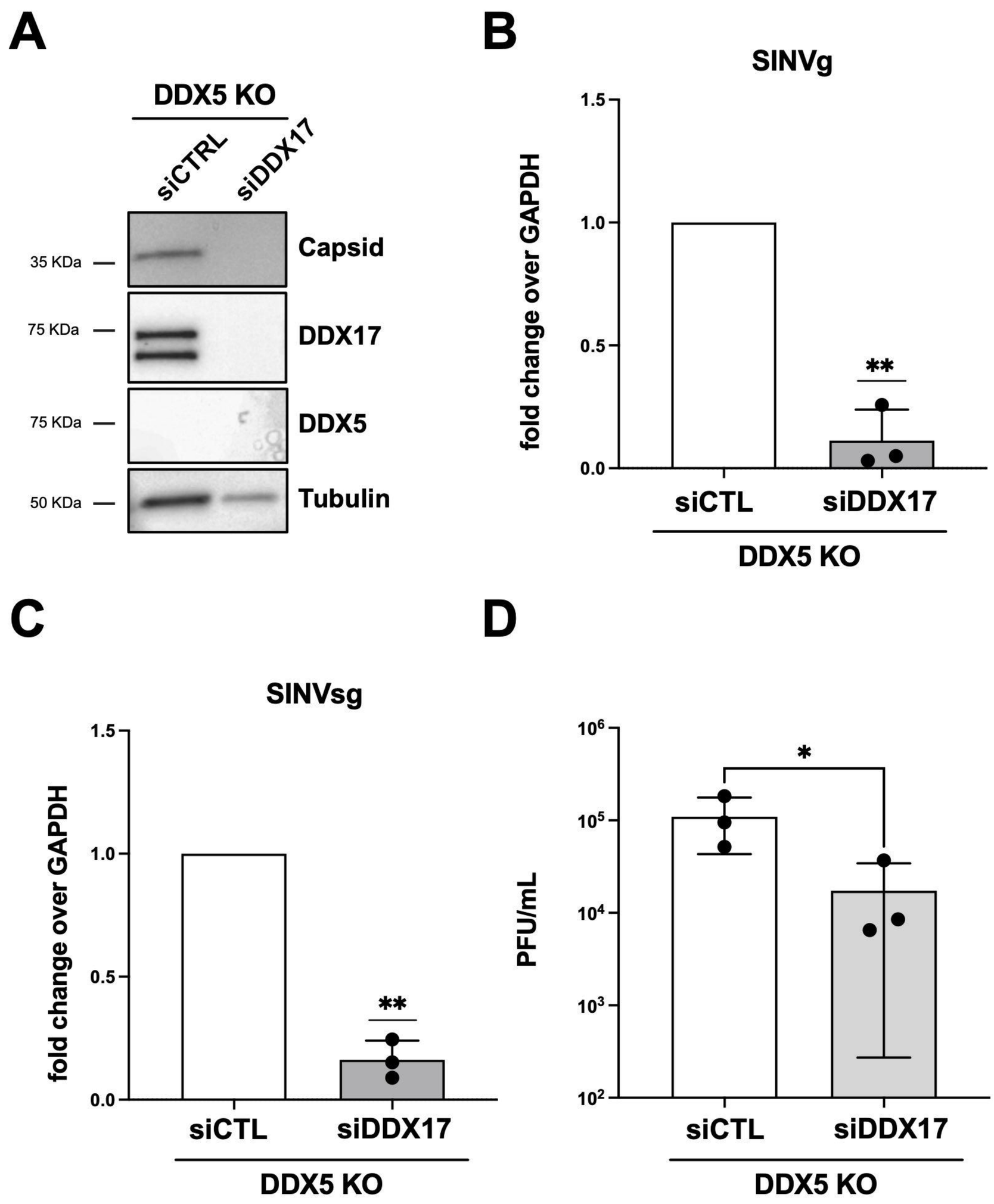
A
DDX5 KO
siCTRL
siDDX17
35 KDa
Capsid
75 KDa
DDX17
75 KDa
DDX5
50 KDa
Tubulin
B
SINVg
fold change over GAPDH
1.5
1.0
0.5
0.0
**
siCTL
siDDX17
DDX5 KO
C
SINVsg
fold change over GAPDH
1.5
1.0
0.5
0.0
**
siCTL
siDDX17
DDX5 KO
D
PFU/mL
10^6
10^5
10^4
10^3
10^2
*
siCTL
siDDX17
DDX5 KO

Figure 6